Shank3 interactions with GKAP and actin help maintain the PSD nanoscale organization

Amy A. Moerkerken, Wouter J. Droogers, Harold D. MacGillavry
Division of Cell Biology, Neurobiology and Biophysics, Utrecht University

Abstract

Synaptic strength is determined by the number of postsynaptic AMPA-type glutamate receptors (AMPARs) that is activated after pre-synaptic neurotransmitter release. This is dependent on the number of AMPARs that is present in the PSD and their positioning relative to the neurotransmitter release site. PSD95 is a scaffolding protein that is involved in recruiting and placing the AMPARs in the PSD. It is organized into nanodomains that increase in number and density upon induction of LTP. These reorganizations were shown to be dependent on the presence of Shank3. Shank3 is a scaffolding protein that interacts with many other PSD scaffolding molecules and links them to the actin cytoskeleton. Elucidating which of the many possible Shank3 interactions underly the re-organization of PSD95 is essential to increase our understanding of synaptic strength and plasticity. Therefore, we used direct Stochastic Optical Reconstruction Microscopy (dSTORM) imaging of endogenously labelled PSD95, combined with re-expression of specific mutated Shank3 variants to determine which Shank3 interactions influence the PSD95 nanoscale distribution. It was found that weakening the connection with GKAP, the protein that links Shank3 to PSD95, leads to an LTP-like reorganization of PSD95. Additionally, the effects of disrupting Shank3/actin mutations were determined, since Shank3 is perfectly positioned to transduce any changes in the dynamic actin cytoskeleton to the upper PSD. Surprisingly, three mutations that disrupt the interaction between Shank3 and F-actin or actin-binding proteins did not influence PSD95 nanoscale organization. Nevertheless, the actin cytoskeleton does play a role in regulating PSD95 nanoscale organization. Treatment and washout of actin depolymerizing drug Latrunculin B (latB) in rat hippocampal neurons led to an increase in the number of PSD95 nanodomains. Additionally, treatment and wash-out of both LatB and Jasplakinolide (Jasp) impaired LTP-induced PSD95 reorganization. Based on these results, it can be hypothesized that the actin cytoskeleton is able to influence the organization of the upper PSD through Shank3. Regulation by the actin cytoskeleton could stabilize and maintain the PSD95 nanoscale distribution. Release of the control of actin on the PSD, either by decoupling Shank3 from PSD95 or by depolymerizing the actin network, allows PSD95 to reorganize.

Layman's summary

Whenever we create a memory or learn a new skill, the information we just acquired is stored within our brain. Our brain is built up of brain cells, which we call neurons. These neurons form many connections with each other, through which they can communicate. This communication occurs through the transfer of electrical signals from one neuron to another. When a neuron needs to communicate with another neuron, an electrical signal is generated. This signal travels through the transmitting neuron to a contact point with the accepting neuron. Each of these contact points between two neurons is called a synapse. At the synapse, the electrical signal causes the release of

chemicals, called neurotransmitters. These neurotransmitters then bind to a receptor on the accepting cell. The binding causes the receptor to open and electrically charged particles flow through. This creates an electric current that can be further transmitted. An important process that allows us to learn, is the strengthening of synapses. When a synapse is strengthened, the receiving cell will create a stronger electrical current in response to the signalling of the transmitting cell. We already know that this stronger response is created by adding extra receptors to the synapse. In this way, the neurotransmitters can open more receptors at once. This results in a larger flow of electrically charged particles and therefore a stronger electrical current. However, it turns out that it is not just the absolute number of receptors that determines the strength of a synapse. The location of the receptors within the synapse is also very important. This is because the neurotransmitters quickly spread and leak away after their release. This means that only those receptors that are located very close to where the neurotransmitters are released, will be opened. In line with these findings, previous studies found that the receptors of the accepting cells are not randomly placed. Instead, they form clusters close to the sites where neurotransmitter is released. On top of that, the density and the number of these receptor clusters increases after the synapse is strengthened. In this study, we wanted to find out how the organization of these receptor clusters comes about and what causes changes in the organization after strengthening of the synapse. We found that there is a structure present within the accepting cells that could keep the receptor clusters in place. This structure is called the actin cytoskeleton. You can picture the actin cytoskeleton as a very flexible and dynamic tree that is constantly growing new branches and breaking down other branches. The actin cytoskeleton binds indirectly to the receptor clusters and keeps them where they are. When the actin cytoskeleton is broken down or when the connection between the cytoskeleton and the receptor clusters is lost, the receptors are no longer kept in place and are free to reorganize. This could be what happens during strengthening of the synapse. By unravelling the mechanisms that cause changes in the communication between our neurons we will better understand how our brains function and we will learn more about brain disorders in which this communication is faulty.

Introduction

The human brain contains many neuronal networks that enable thought processes, learning and memory. The neurons within these networks are highly interconnected. The neuronal axons form synaptic contacts with spines on the dendrites of other neurons. The strength of these synapses is determined by the amplitude of the postsynaptic currents that are evoked by presynaptic neurotransmitter release. Changes in synaptic strength are important for learning and memory formation. Furthermore, it was demonstrated that many neuronal disorders -such as autism spectrum disorder (ASD), schizophrenia and intellectual disabilities- are characterized by defects in synaptic signalling (Bozdagi *et al.,* 2010; Keller *et al.,* 2017; Obi-Nagata *et al.,* 2019). It is therefore of the utmost importance that we increase our understanding of the biological mechanisms that govern synaptic strength and plasticity.

One form of synaptic plasticity is long-term potentiation (LTP), which is the lasting strengthening of a synapse. LTP is mediated by the NMDA-type glutamate receptors (NMDARs). During LTP, the NMDARs are activated and more AMPA-type glutamate receptors (AMPARs) are trafficked into the postsynaptic density (PSD) to enhance the synaptic response (Makino & Malinow, 2009; Hayashi et al.,2000; Shi et al., 1999). However, recent studies have shown that it may not just be the number of AMPARs that determines the strength of a synapse, but also the AMPAR distribution within the PSD.

Computer models demonstrated that glutamate disperses rapidly in the synaptic cleft after release. This results in a swift decrease in glutamate concentration with increasing distance from the release site (Boucher *et al.,* 2010; Raghavachari & Lisman, 2004; Franks *et al.,* 2003). Since AMPARs have a relatively low affinity for glutamate, their activation probability also diminishes with decreasing glutamate concentration (Franks *et al.,* 2003; Raghavachari & Lisman, 2004). In line with these findings, computer simulations showed that adding receptors specifically to nanodomains aligned with presynaptic release sites, enhances synaptic transmission (MacGillavry *et al.,* 2013; Nair *et al.,* 2013). This means that alterations in the positioning of AMPARs could influence synaptic strength and therefore play an important role in synaptic plasticity.

The organization of AMPARs within the PSD is determined by scaffolding proteins, such as PSD95, GKAP and the Shank protein family (Bats *et al.,* 2007; Schnell *et al.,* 2002; Naisbitt *et al.,* 1999). It was determined that these scaffolding proteins and the AMPA receptors are not distributed homogenously throughout the PSD. Instead, they form distinct nanodomains of 75-100 nm in diameter (MacGillavry *et al.,* 2013; Nair, et al., 2013; Broadhead et al., 2016; Fukata *et al.,* 2013; Serweta *et al.,* 2021 unpublished). Interestingly, these postsynaptic nanodomains are aligned with presynaptic release sites (Tang *et al.,* 2016). Furthermore, it was demonstrated that the nanodomain organization of these proteins changes during synaptic plasticity. Long-term depression (LTD) was shown to result in smaller PSD95 nanodomains (Compans *et al.,* 2021). Additionally, Tang *et al.* (2016) and Wiesner *et al.* (2020) observed an increase in the alignment of PSD95 nanodomains with presynaptic nanodomains of scaffolding proteins after LTP induction. In addition to an increase in pre- and postsynaptic alignment, Hruska *et al.* (2018) showed that the number of aligned PSD95 nanodomains also increases during LTP using Stimulated Emission Depletion Microscopy (STED). Our lab has also shown that induction of LTP triggers changes in the organization of these postsynaptic nanodomains. During LTP, PSD95 and GKAP nanodomains increase in number and density and are re-located to the periphery of the PSD (Serweta *et al.,* 2021 unpublished). These findings further strengthen the notion that the subsynaptic distribution of neurotransmitter receptors and scaffolding proteins plays a role in governing synaptic strength and plasticity.

However, the molecular mechanisms that regulate the subsynaptic distribution of PSD proteins remain unknown. In this study we identify the scaffolding protein Shank3 and the actin cytoskeleton as two key molecular players that are involved in the organization of the PSD nano-structure. It is known that actin dynamics are increased during plasticity and that changing actin dynamics abolishes synaptic plasticity (Nakahata & Yasuda, 2018; Okamoto *et al.,* 2004 ; Kim & Lisman, 1999; Krucker *et al.,* 2000). Changes in actin dynamics could therefore be involved in either driving or consolidating LTP-associated changes in the PSD nanostructure. The protein family that links the actin cytoskeleton to the upper layers of the PSD and ultimately to the AMPARs, is the Shank family of scaffolding proteins. This family consists of three isoforms (Shank1-3) that are found in the deeper layers of the PSD. They play an important role in recruiting and crosslinking scaffolding proteins and receptors (Tu *et al.,* 1999; Naisbitt *et al.,* 1999). It has already been demonstrated that Shank proteins are vital for the maintenance of LTP. Electrophysiological recordings indicate that mutation or loss of the Shank genes impairs the neuronal capacity for lasting LTP (Kouser *et al.,* 2013; Bozdagi *et al.,* 2010). On top of that, our lab has shown that simultaneous depletion of all Shank isoforms abolishes the LTP-induced nanoscale reorganization of PSD95. Re-expression of specifically the Shank3 isoform rescued PSD95 reorganization after LTP (Serweta *et al.,* 2021 unpublished). All these findings point to an important role for the Shank proteins, specifically Shank3, in the regulation of the PSD nano-organization.

Shank3 is an incredibly versatile protein. It has many interaction partners, such as other scaffolding proteins, small GTPases, the actin cytoskeleton and multiple actin-binding proteins (Salooma, et al., 2020; Wang *et al.,* 2020**;** Lilja *et al.,* 2017**;** Zeng *et al.,* 2016 MacGillavry, et al., 2016; Sarowar & Grabrucker, 2016). The question remains which of these Shank3 interactions are involved in regulating PSD organization. Therefore, we created four Shank3 mutations to identify the interaction partners that are important for governing the subsynaptic distribution of PSD95. It was found that weakening the interaction between Shank3 and GKAP, which links Shank3 to the upper PSD (Naisbitt *et al.,* 1999; Zeng *et al.,* 2016), induces an increase in PSD95 nanodomain number and density. These results indicate a role for Shank3 in maintaining PSD95 organization through its interaction with GKAP. In addition to the connection between Shank3 and GKAP, its interaction with the actin cytoskeleton was examined. Neither disrupting the direct binding between Shank3 and actin, nor the interaction with ABI1 or cortactin led to any significant changes in subsynaptic PSD95 organization. However, this lack of effect could be due to redundancy between Shank/actin interactions. Lastly, in order to study the effects of changes in actin dynamics on PSD95 organization, cultured rat hippocampal neurons were treated with actin-disrupting drugs Latrunculin B (LatB) and Jasplakinolide (Jasp). Treatment and wash-out of the actin depolymerizing drug LatB resulted in an increase in the number of PSD95 nanodomains. Additionally, treatment and wash-out of both drugs impaired LTP-associated changes in PSD95 nano-organization. All in all, our results indicate that the actin cytoskeleton could be responsible for consolidating and stabilizing the PSD nanoscale organization through its interaction with Shank3. By removing the constraints imposed on the PSD by the actin cytoskeleton, either through breakdown of the actin network itself or by decoupling Shank3 from the PSD, the control mechanisms that maintain PSD95 organization could be removed.

Results

Decoupling Shank3 from the upper PSD leads to LTP-like PSD95 nanoscale reorganization

PSD95 is a scaffolding protein that binds to the postsynaptic membrane through its palmitoylated N-terminus (Craven *et al.,* 1999; El-Husseini *et al.,* 2000). Additionally, it can interact with AMPARs and their auxiliary subunits through its PDZ domain (Bats *et al.,* 2007; Schnell *et al.,* 2002). During LTP, the subsynaptic organization of PSD95 into nanodomains is altered. PSD95 nanodomains increase in number and relative density. The presence of Shank3 within the synapse was proven to be vital for these rearrangements (Serweta *et al.,* 2021, unpublished). Shank3 is linked to PSD95 through the scaffolding protein GKAP. The Shank PDZ-domain can bind to the C-terminal domain of GKAP (Naisbitt *et al.,* 1999). In turn, GKAP interacts via its N-terminus with PSD95, which enables co-clustering of these three scaffolding proteins within the PSD. This means that the interaction between Shank3 and GKAP could be essential for governing PSD95 nanoscale organization.

Removal of the entire Shank3 PDZ domain, abolishes the binding between Shank3 and GKAP (Zeng *et al.,* 2016). However, the Shank3 PDZ domain and its interaction with GKAP are essential for Shank3 synaptic targeting (Sala *et al.* 2001; Zeng *et al.,* 2016). Deletion of this domain will therefore lead to a removal of Shank3 from the PSD, which would disturb many more Shank3 interactions in the PSD, besides its interaction with GKAP. This would make it difficult to specifically identify the role of the Shank3/GKAP interaction in regulating PSD95 nanoscale organization. Furthermore, Shank3 localization within the PSD was shown to be important for synaptic development (Sala *et al.,* 2001). Disrupting Shank3 synaptic targeting might therefore impair the development of synapses. This

could result in an aberrant PSD nanoscale organization that is not directly caused by changes in the interaction between Shank3 and GKAP but rather by a whole-sale disruption of the formation and maturation of the synapse. Fortunately, Zeng *et al.* (2016) demonstrated that, besides the GKAP binding motif in the Shank PDZ domain, a β-hairpin sequence preceding the Shank PDZ domain aids in Shank3 binding to GKAP. Deletion of this sequence does not completely abolish the Shank3/GKAP interaction, but instead only weakens it (Zeng *et al.,* 2016). They also found that the deletion did not impair Shank3 synaptic targeting and spine maturation to the same extend as complete disruption of the Shank3/GKAP interaction.

Therefore, to investigate role of the Shank3/GKAP mutation in regulation of the PSD-nanoscale organization a Shank3 Δβ-hairpin variant was created. The β-hairpin sequence (T543-Y564) was deleted from a pre-existing DNA-construct containing a Shank3 re-expression gene combined with an miRNA based knockdown of all three Shank isoforms (75% knockdown efficiency, MacGillavry *et al.,* 2016). This construct will be referred to as Shank3r Δβ-hairpin.

Weakening the interaction between GKAP and Shank3 does not disrupt Shank3 synaptic targeting or synaptogenesis

Cultured rat hippocampal neurons (day in vitro 4 [DIV4]) were transfected with either Shank3r wildtype (WT) or Δβ-hairpin and a Homer1c-ALFA overexpression construct. Homer1c is a known PSD marker that does not seem to be influenced in its localization and synaptic targeting by Shank3. Therefore, the Homer1c signal was used to identify PSDs within the neurons and the signal was compared to both the Shank3r WT and mutant signal. After transfection, chemical LTP (cLTP) was induced in these neurons on DIV21-24 (Fig.1A).

No significant differences were observed in synaptic targeting of Shank3 between Shank3r WT and Δβ-hairpin. The colocalization of Homer1c and Shank3 was equal between the two Shank3 variants under basal conditions (Control WT= 84.28%; Control Δβ-hairpin=79.69%; ANOVA; Sidak's multiple comparisons test; p=0.81) and after LTP induction (cLTP WT=77.47%; cLTP Δβ-hairpin=83.59%; ANOVA; Sidak's multiple comparisons test; p=0.57) (Fig.1B,C). This is further confirmed by the unaltered Shaft/PSD intensity ratio for the mCherry-Shank3 signal and the unaltered area in which Shank3 is present within the spine (Supplementary Fig.1). This indicates that the Δβ-hairpin mutation does not significantly interfere with Shank3 synaptic targeting. Therefore, any possible effects of the mutation on the PSD95 organization would be caused by the weakening of the GKAP/Shank3 interaction, not by a loss of Shank3 from the spine. Additionally, there is no significant difference in the number of PSDs based on the Homer1c signal in the dendrites of both Shank3r WT expressing neurons and Shank3r Δβ-hairpin expressing neurons under basal conditions (WT=1.69; Δβ-hairpin=1.25; ANOVA; Sidak's multiple comparisons test; p=0.13) and after LTP (WT=1.71; Δβ-hairpin=1.30; ANOVA; Sidak' s multiple comparisons test; p=0.14; Fig.1D). There does seem to be a trend towards a lower number of PSDs per µm dendrite, however this decrease is not significant. Therefore, the Δβ-hairpin mutation does not seem to majorly interfere with the function of Shank3 in synaptogenesis.

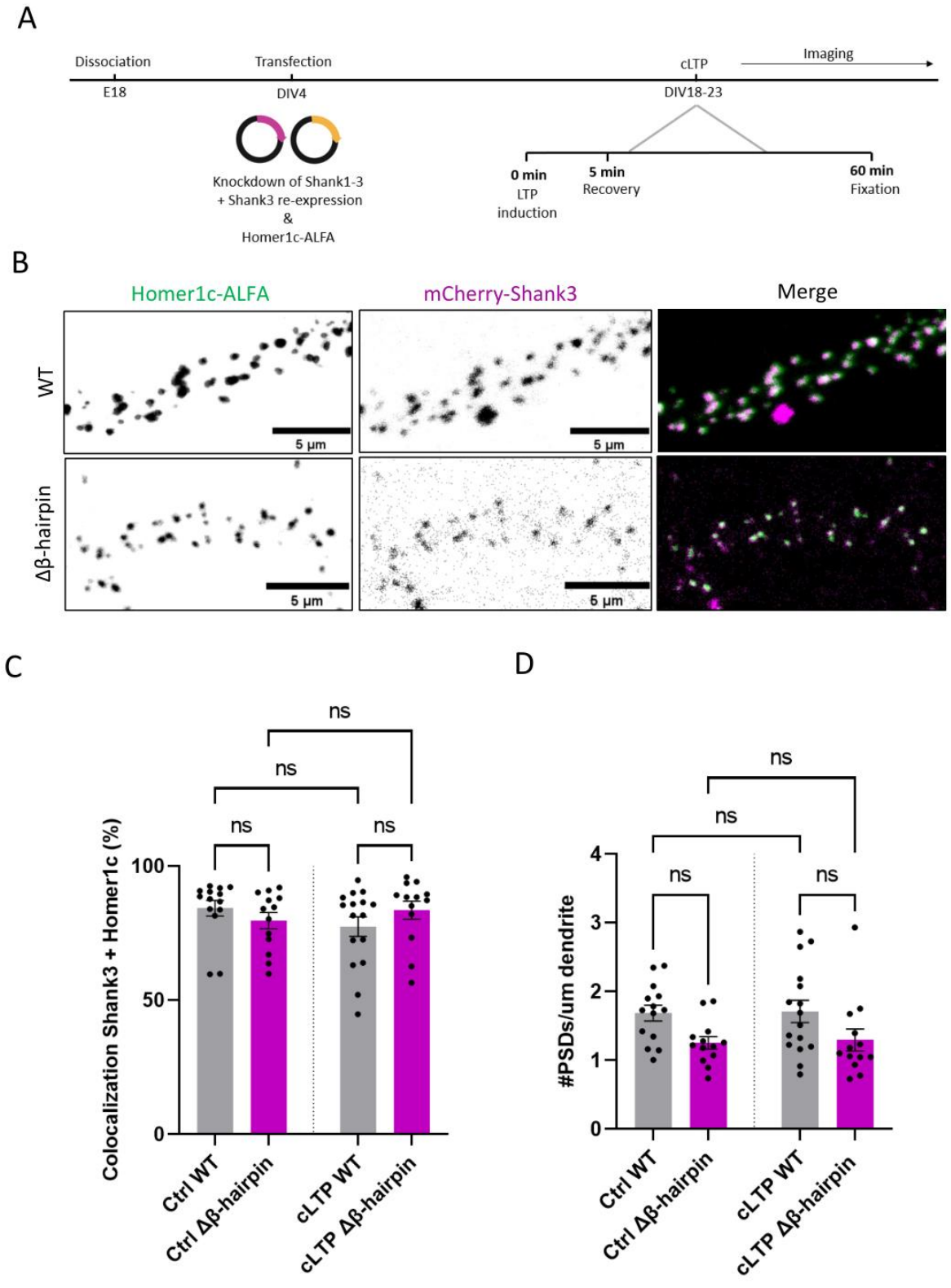

Figure 1. The Shank3 Δβ-hairpin mutation does not disrupt Shank3 synaptic targeting or Shank3-dependent synaptogenesis.

A) Schematic overview of the experimental procedure. Cultured rat hippocampal neurons (DIV4) were transfected with a Shank1-3 knockdown and Shank3 WT or Δβ-hairpin re-expression construct and a Homer1c overexpression construct. On DIV18-23 cLTP was

induced and the Homer1c-ALFA construct was stained with an Atto488-conjugated nanobody. Then, the neurons were fixated and imaged with the Zeiss LSM700 confocal microscope.

B) Representative images of the Homer1c-ALFA and mCherry-Shank3 signal in neuronal dendrites after Shank1-3 knockdown and Shank3 (WT or Δβ-hairpin) re-expression.
C) Mean colocalization of the Shank3 signal with the Homer1c signal within dendrites re-expressing Shank3 WT or Shank3 Δβ-hairpin under basal conditions and after LTP induction. Colocalization represents: (number of Shank3 particles colocalizing with Homer1c particles)/(total number of Homer1c particles) multiplied by 100. No significant differences were found between re-expression of Shank3 WT and Shank3 Δβ-hairpin under basal conditions (WT= 84.28% +/- 2.914%; n=14; Δβ-hairpin=79.69 +/- 3.043%; n=13; ANOVA; Sidak's multiple comparisons test; p=0.81) and after LTP induction (WT=77.47 +/- 3.66%; n=16; Δβ-hairpin=83.59%; +/-3.37%; n=13; ANOVA; Sidak's multiple comparisons test; p=0.57).
D) The mean number of PSDs per µm dendrite of neurons re-expressing Shank3 WT or Shank3 Δβ-hairpin under basal conditions and after LTP induction. PSDs were identified based on the Homer1c-ALFA signal. No significant differences were found between re-expression of Shank3 WT and Shank3 Δβ-hairpin under basal conditions (WT=1.69 +/- 0.115; n=14; Δβ-hairpin=1.25 +/- 0.089; n=13; ANOVA; Sidak's multiple comparisons test; p=0.13) or after LTP induction (WT=1.71 +/- 0.16; n=16; Δβ-hairpin=1.30 +/- 0.16; n=13; ANOVA; Sidak' s multiple comparisons test; p=0.14).

Weakening the interaction between GKAP and Shank3 causes an increase in the number and density of PSD95 nanodomains

After determining that the Δβ-hairpin mutation does not cause any large-scale changes in either Shank3 localization or synaptogenesis, the effects of the mutation on the PSD95 nanoscale organization were studied. Rat hippocampal neurons were transfected with either Shank3r WT or Δβ-hairpin and a PSD95-HaloTag knock-in construct. The knock-in construct was originally created using the CRISPR-Cas9 based ORANGE toolbox (Willems *et al.,* 2020) and it labels endogenous PSD95 with a HaloTag. Subsequently, the PSD95-HaloTag distribution within the PSD was determined under basal conditions and after chemical LTP induction using dSTORM imaging (Fig.2A), followed by a local density based cluster analysis in MATLAB.

Interestingly, expression of Shank3r Δβ-hairpin under basal conditions resulted in an LTP-like PSD95 nanoscale distribution. Compared to the WT, more nanodomains were observed in the PSDs of Shank3r Δβ-hairpin expressing neurons (WT=1.4; Δβ-hairpin=1.6; unpaired t-test; p=0.014). (Fig.2B,D). Furthermore, the relative density of these PSD95 nanodomains was increased compared to the WT (WT=3.5; Δβ-hairpin=4.1; unpaired t-test; p=0.001) (Fig.2C,D). These results indicate that the interaction between Shank3 and GKAP indeed plays a role in governing the subsynaptic PSD95 organization. Furthermore, a weakening of this interaction causes an LTP-like PSD95 nanoscale organization.

The effects of the Δβ-hairpin mutation on LTP-induced reorganization of PSD95, however, were inconclusive. Since LTP did not induce the expected changes in PSD95 nanostructure in neurons re-expressing the Shank3 WT, it is not possible to conclude anything about the effect of the mutation during cLTP (Supplementary Fig.4). This could be due to faulty LTP induction or due to side effects of the control medium.

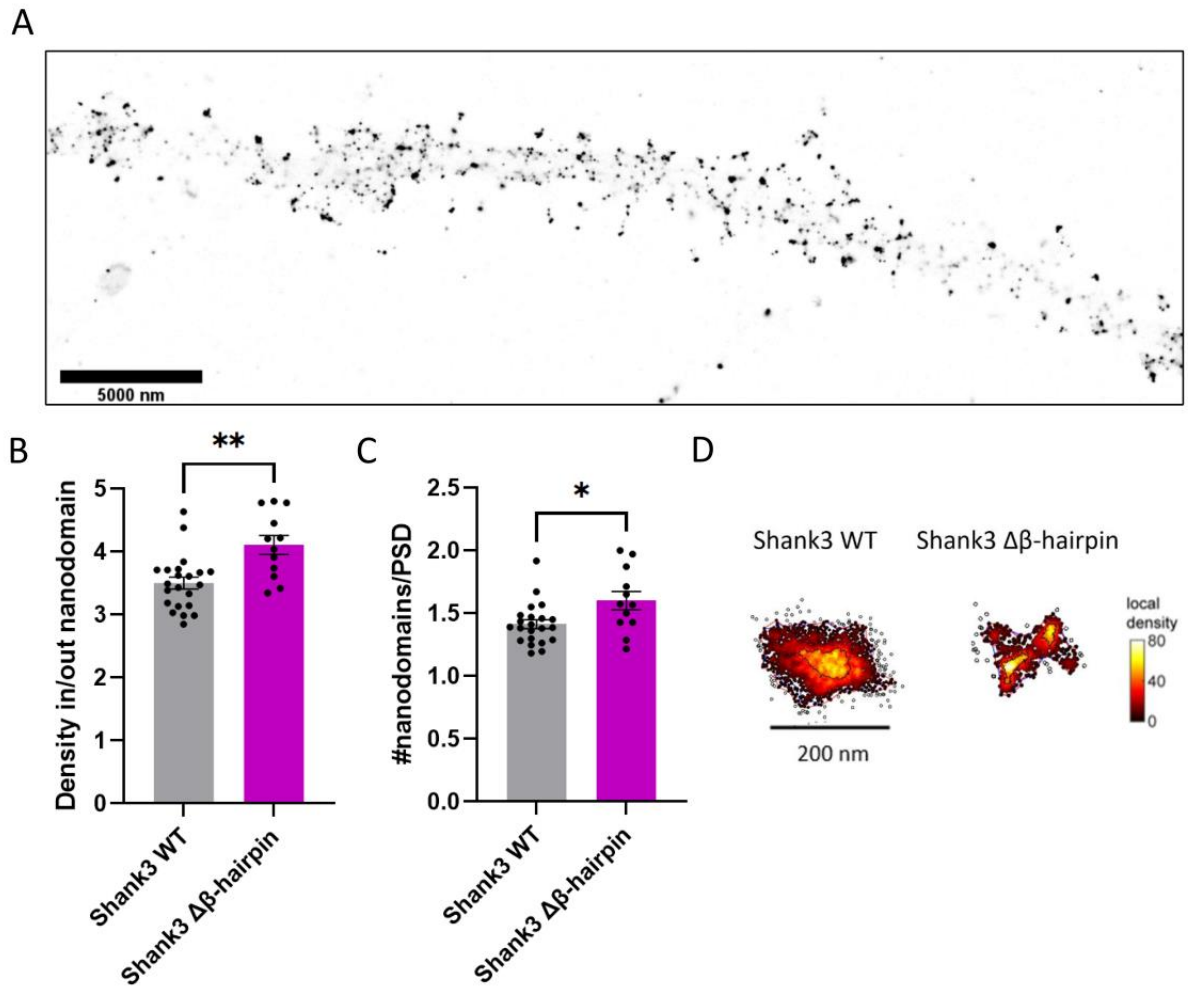

Figure 2. The Shank3 Δβ-hairpin mutation leads to an increase in PSD95 nanodomain number and nanodomain density.

A) Representative dSTORM image of endogenous PSD95-HaloTag signal within a dendrite after knockdown of Shank1-3 and re-expression of Shank3 WT.

B) Mean relative density of PSD95 nanodomains after knockdown of Shank1-3 and re-expression of Shank3 WT or Shank3 Δβ-hairpin. The relative density of PSD95 nanodomains is increased in neurons re-expressing Shank3 Δβ-hairpin compared to the WT (WT=3.5 +/- 0.09; n=22; Δβ-hairpin=4.1 +/- 0.15; n=12; unpaired t-test; p=0.001).

C) Mean number of PSD95 nanodomains per PSD after knockdown of Shank1-3 and re-expression of Shank3 WT or Shank3 Δβ-hairpin. The number of PSD95 nanodomains is increased in neurons re-expressing Shank3 Δβ-hairpin compared to the WT (WT=1.4 +/- 0.035; n=22; Δβ-hairpin=1.6 +/- 0.073; n=12; unpaired t-test; p=0.014).

D) Example images of PSD95 localizations in PSDs from neurons re-expressing Shank3 WT or Shank3 Δβ-hairpin to visualize changes in the PSD95 nano-organization. Nanodomain borders are indicated with a black line.

Disrupting a single interaction between Shank3 and the actin cytoskeleton does not influence PSD95 nanoscale organization

The spine actin cytoskeleton plays an important role in LTP. Actin dynamics are increased during plasticity and blocking actin dynamics abolishes LTP (Fukazawa *et al.,* 2003; Krucker *et al.,* 2000 Fonseca, 2012). Shank3 interacts with the spine actin cytoskeleton and connects it to the upper layers of the PSD. It is therefore possible that the actin network exerts an influence on the organization of PSD95 through its interactions with Shank3 (Salooma *et al.,* 2020, Wang *et al.,* 2020; MacGillavry *et al.,* 2016).

However, there are multiple molecular pathways connecting Shank3 to F-actin. Shank3 binds directly to F-actin and interacts with a multitude of different actin-regulating proteins (Salooma *et al.,* 2020, Wang *et al.,* 2020; MacGillavry *et al.,* 2016). In order to elucidate the relative contributions of specific Shank3/actin interactions, three previously characterized Shank3 mutations were created. These mutations are the Q37A/R38A mutation, the ΔPro mutation and the S685I mutation. The Q37A/R38A mutation is located within the Shank3 SPN domain and it disrupts the direct binding of F-actin to Shank3 (Salooma *et al.,* 2020). Shank3 Δpro lacks the binding motif for the actin nucleation promoting factor cortactin (amino acids 1460-1567) (Uruno *et al.,* 2001; Weaver *et al.,* 2001). A similar deletion was introduced into human Shank2 by MacGillavry *et al.* (2016). They found that Shanks contribute to the recruitment of F-actin and the maintenance of the actin cytoskeleton via retention of cortactin in the spine. The final mutation is Shank3 S685I. Missense mutations at this site are associated with Autism Spectrum Disorders (Wang *et al.,* 2020). S685 is located in the Shank3 proline-rich domain, adjacent to the ABI1 binding motif. Mutation of the S685 residue of Shank3 to a non-phosphorylatable amino acid caused significantly less ABI1 to co-immunoprecipitate with Shank3. Like cortactin, Abl1 is an actin nucleation factor that is part of the Arp2/3 mediated actin nucleation pathway (Wang *et al.,* 2020).

By disrupting these specific connections between Shank3 and the actin cytoskeleton, the relative contributions of these interactions on the subsynaptic organization of PSD scaffolding proteins and AMPARs will become clearer.

Disrupting the interactions between Shank3 and F-actin or actin-interacting proteins cortactin and ABI1 does not influence Shank3 synaptic targeting or synaptogenesis

Cultured rat hippocampal neurons (DIV4) were transfected with the Shank3r WT or mutant (Q37A/R38A, Δpro, S685I) construct and a Homer1c-ALFA overexpression construct. Homer1c was used as a PSD marker. After transfection, cLTP was induced in these neurons on DIV20-23 (Fig.1A).

No significant differences were observed in colocalization of Homer1c with the Shank3r WT compared to the Shank3r mutants Q37A/R38A (WT=86.91%; Q37A/R38A=87.2%; ANOVA; Sidak's multiple comparison test; p=0.997), Δpro (WT=87.87%; Δpro=83.88%; ANOVA; Sidak's multiple comparisons test; p=0.96) and S685I (WT=88.57%; S685I=89.00%; ANOVA; Sidak's multiple comparisons test; p=0.99) under basal conditions (Fig.3 A-B,D-F). Additionally, after LTP-induction colocalization between Shank3 and Homer1c also remained unchanged for the Q37A/R38A (WT=77.15%; Q37A/R38A=83.68%; ANOVA; Sidak's multiple comparison test; p=0.20), Δpro (WT=81.09%; Δpro=79.68%; ANOVA; Sidak's multiple comparisons test; p=0.9991) and S685I mutations (WT=85.12%; S685I=87.75%; ANOVA; Sidak's multiple comparisons test; p=0.60; Fig.3 A-B,D-F). On top of that, no significant differences were found between re-expression of the Shank3 WT and the mutated Shank3 variants in the PSD/shaft ratio for the mCherry-Shank3 fluorenscence

intensity and the area of the Shank3 signal within the PSD (Supplementary Fig.2+3). Based on these results, it can be concluded that Shank3 synaptic targeting is intact for all three mutations. Furthermore, there are no significant changes in the number of PSDs/um dendrite under basal conditions for Q37A/R38A (WT=1.78; Q37A/R38A=1.54; ANOVA; Sidak's multiple comparisons test; p=0.47), Δpro (WT=2.12; Δpro=1.91; ANOVA; Sidak's multiple comparisons test; p=0.77) and S685I (WT=2.05; S685I=1.84; ANOVA; Sidak's multiple comparisons test; p=0.41), nor after LTP induction (WT=1.78; Q37A/R38A=1.54; ANOVA; Sidak's multiple comparisons test; p=0.47; WT=2.04; Δpro=1.66; p=0.20; WT=1.68; S685I=1.50; p=0.47). Therefore, it can be concluded that the Q37A/R38A, Δpro and S685I mutations do not interfere with Shank3 synaptic targeting and the role of Shank3 in synaptogenesis during neuronal development. This means that any possible changes in the PSD nanostructure of neurons expressing the Shank3 Q37A/R38A, Δpro or S685I mutations are due to disturbed Shank3-actin interactions.

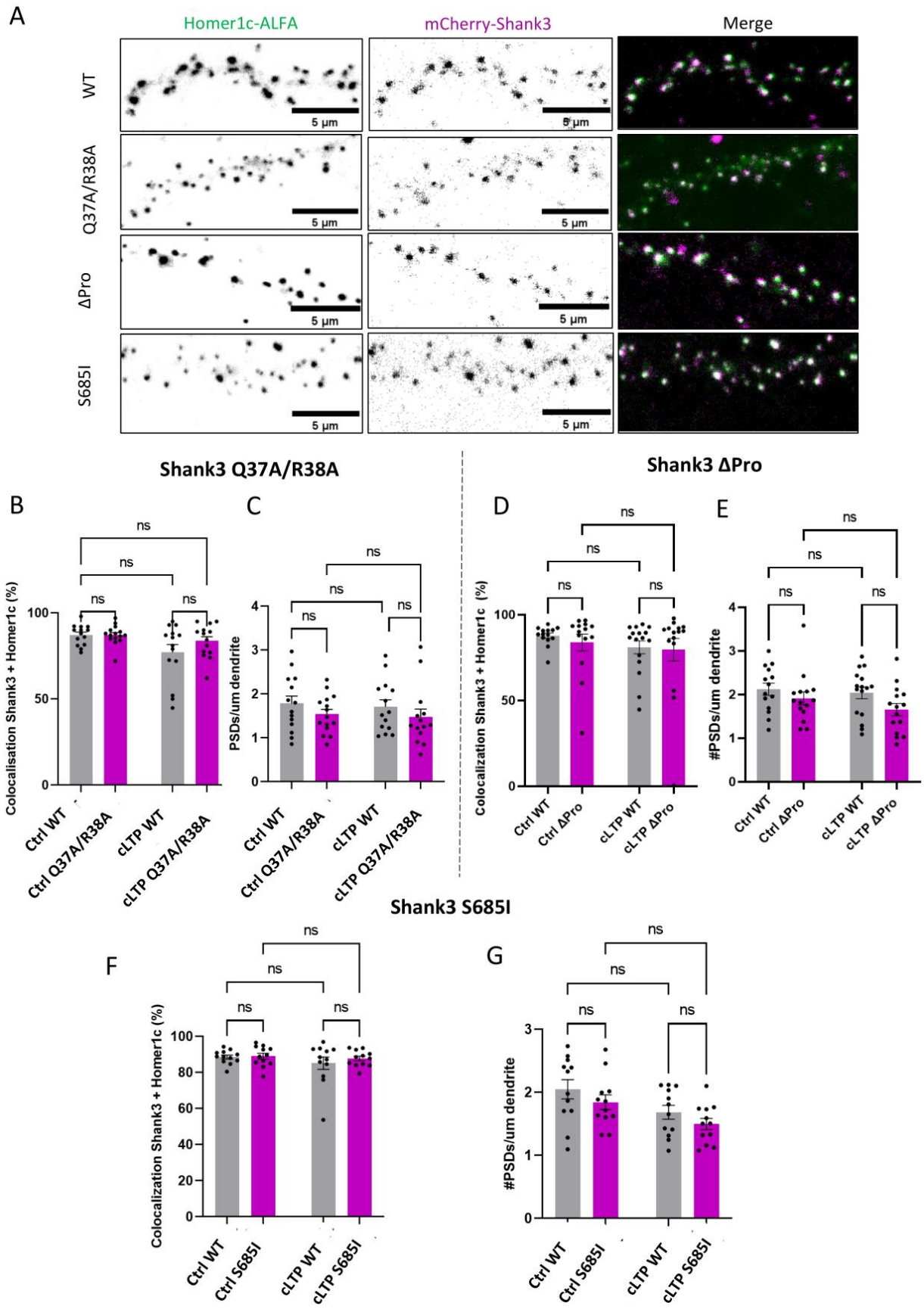

Figure 3. Expression of Shank3 Q37A/R38A, Δpro and S685I does not disrupt Shank3 synaptic targeting or the number of PSDs.

A. Representative images of neuronal dendrites after knockdown of all Shank isoforms and re-expression of Shank3 WT, Shank3 Q37A/R38A, Shank3 Δpro or Shank3 S68I under basal conditions. The cells were co-transfected with Homer1c-ALFA as a PSD marker. Shank3 is labelled with mCherry and Homer1c-ALFA is stained with an anti-ALFA Atto488 nanobody.
B. Mean colocalization of the mCherry-Shank3 signal with the Homer1c signal within dendrites re-expressing Shank3 WT or Shank3 Q37A/R38A under basal conditions and after LTP induction. Colocalization represents: (number of Shank3 particles colocalizing with Homer1c particles)/(total number of Homer1c particles) multiplied by 100. No significant differences were found between re-expression of Shank3 WT and Shank3 Q37A/R38A under basal conditions (WT=86.91 +/- 1.67%; n=13; Q37A/R38A=87.2 +/- 1.45%; n=15; ANOVA; Sidak's multiple comparisons test; p=0.997) or after LTP (WT=77.15 +/- 4.50%; n=14; Q37A/R38A=83.68% +/-2.56%; n=14; ANOVA; Sidak's multiple comparison test; p=0.20).
C. The mean number of PSDs per µm dendrite. Based on the number of Homer1c-ALFA punctae in neurons re-expressing Shank3 WT or Shank3 Q37A/R38A under basal conditions and after LTP induction. No significant differences were found between re-expression of Shank3 WT and Shank3 Q37A/R38A under basal conditions (WT=1.78 +/- 0.17; n=14; Q37A/R38A=1.54 +/- 0.11; n=15; ANOVA; Sidak's multiple comparisons test; p=0.47) and after LTP induction (WT=1.71 +/-0.16; n=14; Q37A/R38A=1.47 +/- 0.18; n=14; ANOVA; Sidak's multiple comparisons test; p=0.51).
D. Mean colocalization of the mCherry-Shank3 signal with the Homer1c signal within dendrites re-expressing Shank3 WT or Shank3 ΔPro under basal conditions and after LTP induction. Colocalization represents (number of Shank3 particles colocalizing with Homer1c particles)/(total number of Homer1c particles) multiplied by 100. No significant differences were found between re-expression of Shank3 WT and Shank3 ΔPro under basal conditions (WT=87.87 +/- 1.50%; n=14; ΔPro=83.88 +/- 4.89%; n=14; ANOVA; Sidak's multiple comparisons test; p=0.96) or after LTP induction (WT=81.09 +/-3.75%; n=16; ΔPro=79.68 +/- 3.75%; n=15; ANOVA; Sidak's multiple comparisons test; p=0.9991).
E. The mean number of PSDs per µm dendrite. Based on the number Homer1c-ALFA punctae in neurons re-expressing Shank3 WT or Shank3 ΔPro under basal conditions (WT=2.12 +/- 0.14; n=14; ΔPro=1.91 +/- 0.15; n=14; ANOVA; Sidak's multiple comparisons test; p=0.77) and after LTP induction (WT=2.04 +/- 0.14; n=16; ΔPro=1.66 +/- 0.14; n=15; ANOVA; Sidak's multiple comparisons test; p=0.20). No significant differences were found between re-expression of Shank3 WT and Shank3 ΔPro.
F. Mean colocalization of the mCherry-Shank3 signal with the Homer1c signal within dendrites re-expressing Shank3 WT or Shank3 S685I under basal conditions (WT=88.57 +/- 1.09%; n=12; S685I=89.00 +/- 1.63%; n=12; ANOVA; Sidak's multiple comparisons test; p=0.99) and after LTP induction (WT=85.12 +/- 3.38%; n=12; S685I=87.75 +/- 1.28%; n=12; ANOVA; Sidak's multiple comparisons test; p=0.60). Colocalization represents (number of Shank3 particles colocalizing with Homer1c particles)/(total number of Homer1c particles) multiplied by 100. No significant differences were found between re-expression of Shank3 WT and Shank3 S685I.
G. The mean number of PSDs per µm dendrite. Based on the number Homer1c-ALFA punctae in neurons re-expressing Shank3 WT or Shank3 S685I under basal conditions (WT=2.05 +/- 0.15; n=12; S685I=1.84 +/- 0.12; n=12; ANOVA; Sidak's multiple comparisons test; p=0.41) and after LTP induction (WT=1.68 +/- 0.11; n=12; S685I=1.50 +/- 0.11; n=12; ANOVA; Sidak's multiple comparisons test; p=0.47). No significant differences were found between re-expression of Shank3 WT and Shank3 S685I.

Disturbing a single interaction between Shank3 and the actin cytoskeleton does not influence PSD95 nanoscale organization

To determine if Shank3-actin interactions play a role in determining PSD95 nanostructure, the subsynaptic distribution of endogenous PSD95 was determined in neurons expressing Shank3r WT and Shank3r Q37A/R38A, Shank3 ΔPro or Shank3 S685I. Rat hippocampal neurons were transfected with Shank3r WT or one of the Shank3r mutant constructs and the ORANGE PSD95-HaloTag knock-in construct. On DIV20-23, cLTP was induced in these neurons. Subsequently, the organization of PSD95-HaloTag within the PSD was determined using dSTORM imaging (Fig.2A) followed by a local density based cluster analysis in MATLAB.

Interestingly, expression of the three mutations did not lead to significant changes in PSD95 distribution. The mean number of nanodomains per PSD in neurons expressing Shank3r Q37A/R38A (WT=1.52; Q37A/R38A=1.43; unpaired t-test; p=0.56), ΔPro (WT=1.52; ΔPro=1.40; n=18; unpaired t-test; p=0.1) and S685I (WT=1.46; S685I=1.60; unpaired t-test; p=0.051) was not significantly different from neurons expressing Shank3r WT. Additionally, the relative density of PSD95 within these nanodomains is also equal between the Shank3r mutants Q37A/R38A (WT=3.91; Q37A/R38A=3.52; unpaired t-test; p=0.10), ΔPro (WT=3.92; ΔPro=3.62; unpaired t-test, p=0.21) or S685I (WT=3.69; S685I=3.92; unpaired t-test; p=0.24) and Shank3r WT expressing neurons (Fig. 4B,DF). It can therefore be concluded that disrupting the interactions ofShank3 with F-actin, cortactin and ABI1 do not significantly influence PSD95 organization within the PSD. However, even though the interactions between Shank3 and F-actin, cortactin and ABI1 do not seem to play a role in PSD nano-organization under basal conditions, they could still be important for PSD95 reorganization during LTP. Unfortunately, the effects of the Shank3 Q37A/R38A, ΔPro and S685I mutations on LTP-induced reorganization of PSD95 were inconclusive. LTP did not induce the characteristic changes in PSD95 nanostructure in neurons re-expressing Shank3 WT (Supplementary Fig.5). Therefore, it is not possible to conclude anything about the effect of these Shank3 mutations on PSD95 nanostructure during LTP.

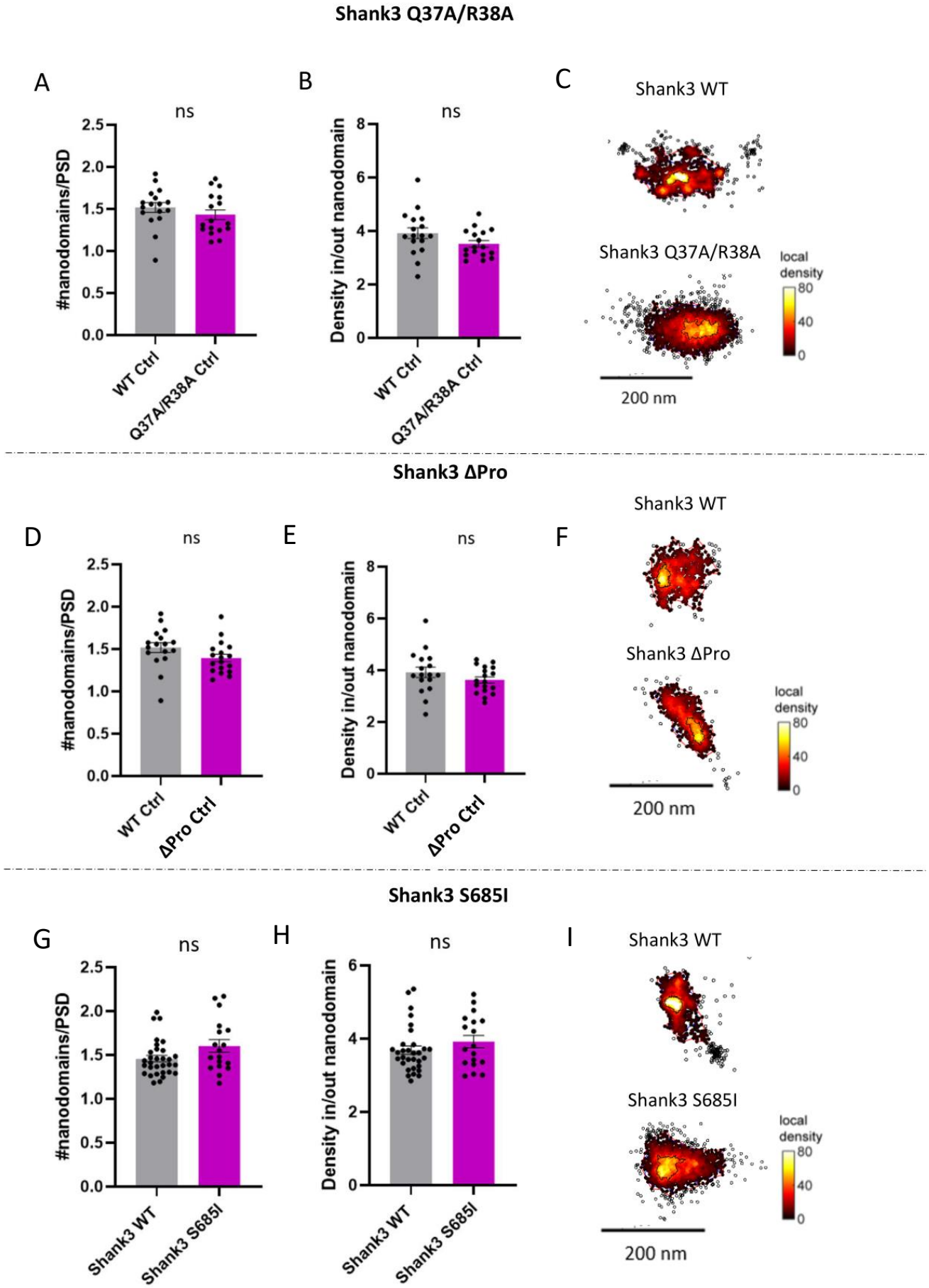
Shank3 Q37A/R38A
A
ns
#nanodomains/PSD
WT Ctrl
Q37A/R38A Ctrl
B
ns
Density in/out nanodomain
WT Ctrl
Q37A/R38A Ctrl
C
Shank3 WT
Shank3 Q37A/R38A
local density
80
40
0
200 nm
Shank3 ΔPro
D
ns
#nanodomains/PSD
WT Ctrl
ΔPro Ctrl
E
ns
Density in/out nanodomain
WT Ctrl
ΔPro Ctrl
F
Shank3 WT
Shank3 ΔPro
local density
80
40
0
200 nm
Shank3 S685I
G
ns
#nanodomains/PSD
Shank3 WT
Shank3 S685I
H
ns
Density in/out nanodomain
Shank3 WT
Shank3 S685I
I
Shank3 WT
Shank3 S685I
local density
80
40
0
200 nm

Figure 4. Shank3 Q37A/R38A, ΔPro and S685I mutations do not cause changes in the number and density of PSD95 nanodomains under basal conditions.

A. Mean number of PSD95 nanodomains per PSD after knockdown of Shank1-3 and re-expression of Shank3 WT or Shank3 Q37A/R38A. No significant differences were found in the number of nanodomains per PSD for the Q37A/R38A condition compared to the WT (WT=1.52 +/- 0.06; n=17; Q37A/R38A=1.43 +/- 0.06; n=17; unpaired t-test; p=0.30).
B. Mean relative density of PSD95 nanodomains after knockdown of Shank1-3 and re-expression of Shank3 WT or Shank3 Q37A/R38A. No changes were found in the relative density for the Q37A/R38A condition compared to the WT control (WT=3.91 +/- 0.2; n=17; Q37A/R38A=3.52 +/- 0.13; n=17; unpaired t-test; p=0.10).
C. Example images of PSD95 localizations in PSDs from neurons re-expressing Shank3 WT or Shank3 Q37A/R38A illustrate that there are no significant differences in the PSD95 nano-organization. Nanodomain borders are indicated with a black line.
D. Mean number of PSD95 nanodomains per PSD after knockdown of Shank1-3 and re-expression of Shank3 WT or Shank3 ΔPro. No significant differences were found in the number of nanodomains per PSD for the ΔPro condition compared to the WT (WT=1.52 +/- 0.06; n=17; ΔPro=1.40 +/- 0.044; n=18; unpaired t-test; p=0.1).
E. Mean relative density of PSD95 nanodomains after knockdown of Shank1-3 and re-expression of Shank3 WT or Shank3 ΔPro. No changes were found in the relative density for the ΔPro condition compared to the control (WT=3.92 +/- 0.20; n=17; ΔPro=3.62 +/- 0.12; n=18; unpaired t-test, p=0.21).
F. Example images of PSD95 localizations in PSDs from neurons re-expressing Shank3 WT or Shank3 ΔPro show that there are no significant differences in the PSD95 nano-organization. Nanodomain borders are indicated with a black line.
G. Mean number of PSD95 nanodomains per PSD after knockdown of Shank1-3 and re-expression of Shank3 WT or Shank3 S685I. No significant differences were found in the number of nanodomains per PSD for the S685I condition compared to the WT (WT=1.46 +/- 0.04; n=31; S685I=1.60 +/- 0.037; n=18; unpaired t-test; p=0.051).
H. Mean relative density of PSD95 nanodomains after knockdown of Shank1-3 and re-expression of Shank3 WT or Shank3 S685I. No changes were found in the relative density for the S685I condition compared to the control (WT=3.69 +/- 0.11; n=31; S685I=3.92 +/- 0.17; n=18; unpaired t-test; p=0.24).
I. Example images of PSD95 localizations in PSDs from neurons re-expressing Shank3 WT or Shank3 S685I illustrate that there are no significant differences in the PSD95 nano-organization. Nanodomain borders are indicated with a black line.

Altering the dynamics of the actin cytoskeleton induces changes in PSD95 nanoscale organization

LTP-induction is dependent on dynamic actin filaments within the spine (Krucker *et al.,* 2000 Fonseca, 2012). Almost directly after stimulation, the spine head expands, F-actin accumulates and actin severing proteins are recruited to the spine while actin stabilizing proteins are removed (Bosch *et al.,* 2014; Mizui *et al.,* 2014). These changes in the actin dynamics could play a role in regulating PSD reorganization during LTP. For example by inducing changes in the PSD95 organization through the interaction with Shank3 or by stabilizing the new LTP-induced organization of PSD95 in order to ensure lasting maintenance of LTP. To determine whether actin dynamics influence PSD95 nanoscale

organization, neurons were treated with actin disrupting drugs Latrunculin B (LatB) and Jasplakinolide (Jasp) under basal conditions or during LTP induction, followed by recovery and wash-out of the drugs.

Actin dynamics influence the PSD95 nanoscale organization

To determine the effect of disrupting the dynamics of the actin cytoskeleton on the nanoscale organization of PSD95, neurons were treated with actin disrupting drugs under basal conditions. Cultured rat hippocampal neurons (DIV4) were transfected with the ORANGE PSD95-HaloTag knock-in construct. At DIV20-23 the neurons were transferred to control medium containing 1 µM LatB or 0.2 µM Jasp as treatment or 0.2 µL DMSO in control conditions for 5 minutes. LatB induces depolymerization of the actin network by sequestering free actin monomers and thereby blocking their incorporation in actin filaments. This results in net depolymerization (Morton *et al.,* 2000). Jasp stabilizes the actin network. It blocks depolymerization, but does still allow for slight polymerization (Holzinger, 2001). After 5 minutes, the cells were either fixated or transferred to drug-free control medium for 55 minutes, allowing for recovery and wash-out of the drugs. After wash-out, these neurons were also fixated. Subsequently, the PSD95 nanoscale organization was determined using dSTORM imaging followed by a local-density based cluster analysis in MATLAB (Fig.5A).

Immediately after the 5-minutes of drug-treatment, no differences could be observed in the number of PSD95 nanodomains between the non-treated cells and the cells treated with LatB (DMSO=1.43; LatB=1.39; ANOVA; Sidak's multiple comparisons test; p=0.97) or Jasp (DMSO=1.43; Jasp=1.32; ANOVA; Sidak's multiple comparisons test; p=0.63) (Fig.5B). The relative density of the PSD95 nanodomains also remained unchanged after treatment with LatB (DMSO=3.52; LatB=3.52; ANOVA; Sidak's multiple comparisons test; p>0.9999) and Jasp (DMSO=3.52; n=8; Jasp=3.32; n=12; p=0.63; Fig.5E). However, changes in the subsynaptic PSD95 organization did start to appear after 55 minutes of wash-out. Specifically, the number of PSD95 nanodomains per PSD was increased in neurons after LatB treatment plus wash-out compared to non-treated neurons (DMSO=1.39; LatB=1.61; ANOVA; Sidak's multiple comparisons test; p=0.037; Fig.5C). For Jasp treatment plus wash-out, the number of nanodomains remained the same as the control group (DMSO=1.39; Jasp=1.35; ANOVA; Sidak's multiple comparisons test; p=0.82; Fig.5C). The relative density of the PSD95 nanodomains was unaffected by either LatB treatment plus wash-out (DMSO=3.42; LatB=3.64; ANOVA; Sidak's multiple comparisons test; p=0.68) or Jasp treatment plus wash-out (DMSO=3.42; Jasp=3.62; ANOVA; Sidak's multiple comparisons test; p=0.69) (Fig.5F). This means that depolymerization of the actin network by LatB has a delayed effect on PSD95 nanoscale organization. Strikingly, depolymerizing the actin network leads to an increase in the number of nanodomains.

However, it is not known exactly what the effects of LatB and Jasp wash-out are on the dynamics of the actin network. It is possible that any effects on the PSD95 nanostructure after wash-out are not simply delayed effects of the drugs themselves, but instead reflect a compensatory response of the neuron to the exposure to the drugs. Therefore, rat hippocampal neurons (DIV4) were transfected with an ORANGE β-actin knock-in construct that labels endogenous G-actin and F-actin with a HaloTag. Subsequently, these cells (DIV20-23) were live-cell imaged during LatB and Jasp treatment and wash-out to determine what happens to the dynamics of the actin network. Unfortunately, the results were inconclusive due to an insufficient amount of data (Supplementary Fig.6).

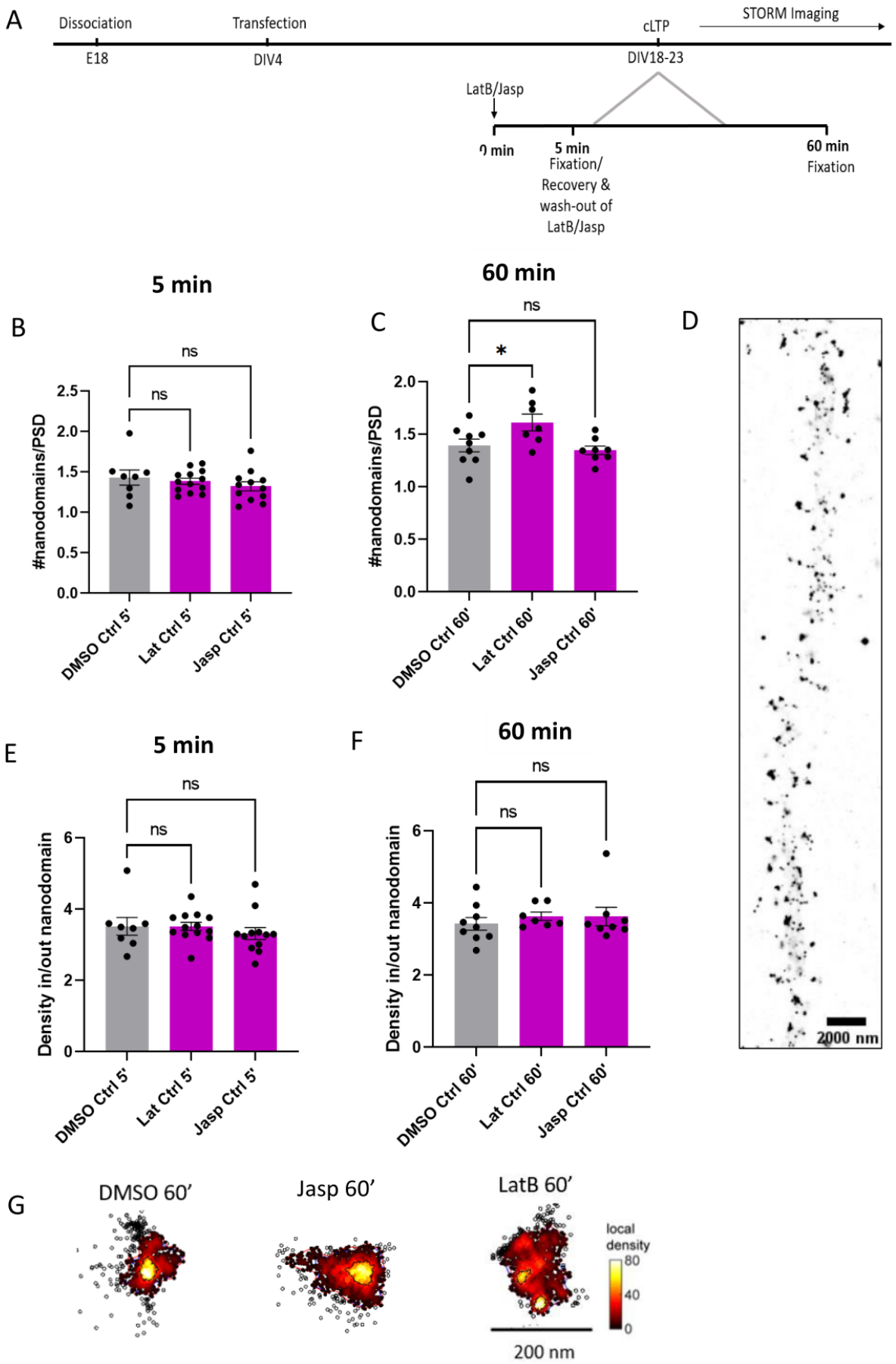
A
Dissociation
E18
Transfection
DIV4
cLTP
DIV18-23
STORM Imaging
LatB/Jasp
0 min
5 min
Fixation/
Recovery &
wash-out of
LatB/Jasp
60 min
Fixation
B
5 min
#nanodomains/PSD
ns
ns
DMSO Ctrl 5'
Lat Ctrl 5'
Jasp Ctrl 5'
C
60 min
#nanodomains/PSD
ns
*
DMSO Ctrl 60'
Lat Ctrl 60'
Jasp Ctrl 60'
D
2000 nm
E
5 min
Density in/out nanodomain
ns
ns
DMSO Ctrl 5'
Lat Ctrl 5'
Jasp Ctrl 5'
F
60 min
Density in/out nanodomain
ns
ns
DMSO Ctrl 60'
Lat Ctrl 60'
Jasp Ctrl 60'
G
DMSO 60'
Jasp 60'
LatB 60'
local
density
80
40
0
200 nm

Figure 5. Treatment with LatB leads to an increase in the number of PSD95 nanodomains, while Jasp treatment has no effect on PSD95 nanoscale organization.

A. Schematic overview of the experimental procedure. Cultured rat hippocampal neurons were transfected with the ORANGE PSD95-Halo knock-in construct on DIV4. Then, on DIV21-23 PSD95-HaloTag was labelled and the cells were transferred to E5 medium containing 1 µM LatB, 0.2 µM Jasp or 0.2 µL DMSO (control) for 5 minutes. After 5 minutes, the cells were directly fixated or they transferred to normal E5 for 55 minutes prior to fixation. After fixation, PSD95-HaloTag was imaged using dSTORM.
B. Mean number of PSD95 nanodomains in the PSDs of neurons fixated directly after 5 minutes of treatment with 1 µM LatB, 0.2 µM Jasp or DMSO (control). There are no significant differences in the number of nanodomains between DMSO treatment and LatB (DMSO=1.43 +/- 0.09; n=8; LatB=1.39 +/- 0.04; n=13; ANOVA; Sidak's multiple comparisons test; p=0.97) or Jasp (DMSO=1.43 +/- 0.09; n=8; Jasp=1.32 +/- 0.06; n=12; ANOVA; Sidak's multiple comparisons test; p=0.63).
C. Mean number of PSD95 nanodomains in neurons fixated after 5 minutes of 1 µM LatB, 0.2 µM Jasp or DMSO treatment followed by 55 minutes of wash-out. The number of PSD95 nanodomains is significantly increased for the LatB condition compared to the control (DMSO=1.39 +/- 0.06; n=9; LatB=1.61 +/- 0.08; n=8; ANOVA; Sidak's multiple comparisons test; p=0.037). There is no significant change in the number of nanodomains after Jasp treatment plus wash-out compared to the control (DMSO=1.39 +/- 0.06; n=9; Jasp=1.35 +/- 0.04; n=8; ANOVA; Sidak's multiple comparisons test; p=0.82).
D. Representative dSTORM image of endogenous PSD95-HaloTag signal within a dendrite after receiving the control treatment with DMSO.
E. Mean relative density of PSD95 nanodomains in the PSDs of neurons fixated directly after 5 minutes of treatment with 1 µM LatB, 0.2 µM Jasp or DMSO (control). There are no significant differences in the relative density between DMSO treatment and LatB (DMSO=3.52 +/- 0.25; n=8; LatB=3.52 +/- 0.11; n=13; ANOVA; Sidak's multiple comparisons test; p>0.9999) or Jasp (DMSO=3.52 +/- 0.25; n=8; Jasp=3.32 +/- 0.17; n=12; ANOVA; Sidak's multiple comparisons test; p=0.63).
F. Mean relative density of PSD95 nanodomains in the PSDs of neurons fixated after 5 minutes of 1 µM LatB, 0.2 µM Jasp or DMSO treatment followed by 55 minutes of wash-out. There are no significant differences in the relative density between DMSO treatment and LatB (DMSO=3.42 +/- 0.17; n=9; LatB=3.64 +/- 0.12; n=7; ANOVA; Sidak's multiple comparisons test; p=0.68) or Jasp (DMSO=3.42 +/- 0.17; n=9; Jasp=3.62 +/- 0.26; n=8; ANOVA; Sidak's multiple comparisons test; p=0.69).
G. Representative nano-scale distribution of PSD95 within the PSD after treatment with 1 µM LatB plus wash-out, 0.2 µM Jasp plus wash-out or 2 µL DMSO treatment plus wash-out. Nanodomain borders are indicated with a black line. The number of nanodomains per PSD is increased in the LatB group compared to the DMSO group.

Disrupting actin dynamics interferes with LTP-induced PSD95 reorganization

Now that it was shown that changes in actin dynamics are indeed capable of influencing PSD95 nanoscale organization, it is time to investigate the role of actin specifically in LTP-induced PSD95 reorganization. Rat hippocampal neurons were transfected with the ORANGE PSD95-HaloTag knock-in on DIV4.. Subsequently, chemical LTP was induced (DIV20-23). 2 µL DMSO, 1 µM LatB or 0.2 µM Jasp were added to the chemical LTP medium. After 5 minutes of LTP-induction and drug treatment, the cells were transferred to control medium without any of the drugs to recover. Finally, the PSD95

nanoscale organization was determined using dSTORM imaging followed by a local density based cluster analysis in MATLAB (Fig.6A).

After treatment with LatB or Jasp followed by wash-out, PSD95 reorganization is diminished or absent. For both LatB and Jasp treatment, there no longer is any increase in the number of PSD95 nanodomains after LTP induction (Fig.6B). Surprisingly, the increase in the number of nanodomains is also not significant for the control DMSO treatment. However, there is a trend visible towards a larger number of nanodomains per PSD (Control=1.39; cLTP=1.57; ANOVA; Sidak's multiple comparisons test; p=0.95). For both LatB (Control=1.61; cLTP=1.48; ANOVA; Sidak's multiple comparisons test; p=0.63) and Jasp treatment (Control=1.35; n=8; cLTP=1.40; n=11; ANOVA; Sidak' s multiple comparisons test; p=0.997), there is no longer any increase in the number of PSD95 nanodomains after LTP induction (Fig.6B). The same is true for the relative density of the PSD95 nanodomains. For the control condition there is a trend towards denser PSD95 nanodomains (Control=3.42; cLTP=3.75; ANOVA; Sidak's multiple comparisons test; p=0.46) (Fig.6C). This trend is smaller after treatment and wash-out of LatB (Control=3.64; cLTP=3.74; ANOVA; Sidak's multiple comparisons test; p=0.97) (Fig.6C) and the trend is reversed after treatment and wash-out of Jasp (Control=3.62; cLTP=3.49; ANOVA; Sidak' s multiple comparisons test; p=0.94) (Fig.6C). This means that changing actin dynamics could interfere with LTP-induced PSD95 reorganization. These results therefore point to a role for actin dynamics in PSD reorganization during LTP.

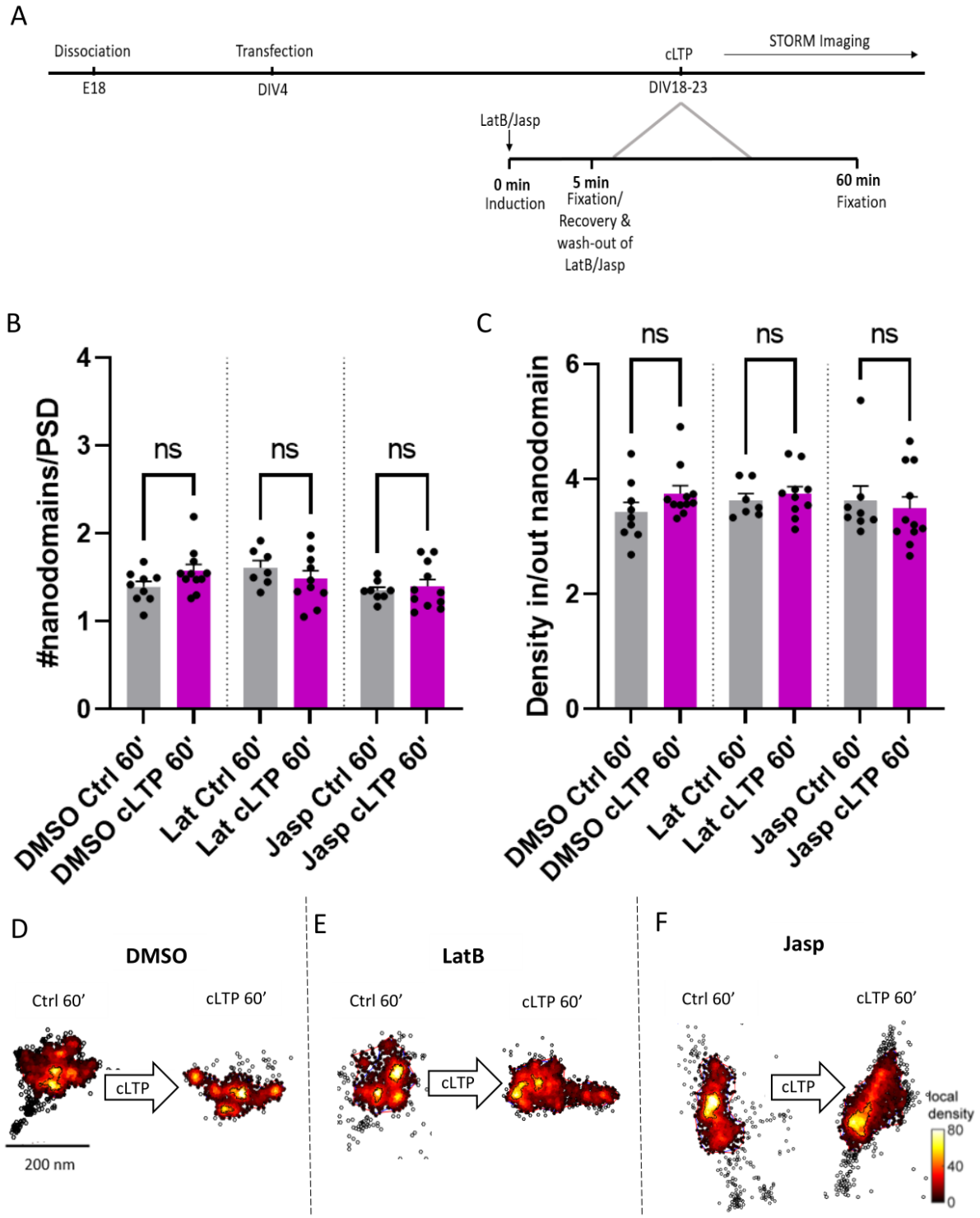

Figure 6. Changing actin dynamics interferes with LTP-induced PSD95 reorganization.

A. Overview experimental set-up. Cultured rat hippocampal neurons were transfected with ORANGE PSD-95 HaloTag on DIV4. Then, they were live-cell labelled with Halo-ligand Janelia Fluor 646, followed by LTP induction in the presence of 2 µL DMSO, 1 µM LatB or 0.2 µM Jasp. After induction, the cells were placed in normal E5 medium in the absence of the drugs to recover. The cells were fixated and imaged using dSTORM.

B. Mean number of PSD95 nanodomains in neurons fixated after 5 minutes of LTP induction in the presence of 1 µM LatB, 0.2 µM Jasp or DMSO, followed by 55 minutes of recovery and

drug wash-out. For the control condition), a trend towards more nanodomains per PSD is visible (Control=1.39 +/- 0.06; n=9; cLTP=1.57 +/- 0.08; n=11; ANOVA; Sidak's multiple comparisons test; p=0.95). However, there is no trend towards increase for the number of nanodomains after LatB treatment plus wash-out (Control=1.61 +/- 0.08; n=7; cLTP=1.48 +/- 0.09; n=10 ANOVA; Sidak's multiple comparisons test; p=0.63) or Jasp treatment plus wash-out (Control=1.35 +/- 0.04; n=8; cLTP=1.40 +/- 0.08; n=11; ANOVA; Sidak' s multiple comparisons test; p=0.997).

C. Mean relative density of PSD95 nanodomains in the PSDs of neurons fixated after 5 minutes of LTP induction in the presence of 1 µM LatB, 0.2 µM Jasp or DMSO, followed by 55 minutes of wash-out. The PSDs in neurons of the control group show a trend towards denser nanodomains (Control=3.42 +/- 0.17; n=9; cLTP=3.75 +/- 0.14; n=11; ANOVA; Sidak's multiple comparisons test; p=0.46). There is no such trend after LatB treatment plus wash-out (Control=3.64 +/- 0.12; n=7; cLTP=3.74 +/- 0.13; n=10; ANOVA; Sidak's multiple comparisons test; p=0.97) or Jasp treatment plus wash-out (Control=3.62 +/- 0.26; n=8; cLTP=3.49 +/- 0.20; n=11; ANOVA; Sidak' s multiple comparisons test; p=0.94).
D. Example images of PSDs from neurons that were treated with 2 µL DMSO followed by wash-out, under basal conditions and after LTP-induction. Nanodomain borders are indicated by a black line. There seems to be a trend towards an increase in PSD95 nanodomain number and density after LTP-induction.
E. Example images of the PSD95 distribution in PSDs from neurons that were treated with 1 µM LatB followed by wash-out followed by wash-out, under basal conditions and after LTP-induction. LatB treatment seems to interfere with the LTP-induced PSD95 nanoscale organization.
F. Example images of the PSD95 distribution in PSDs from neurons that were treated with 0.2 µM Jasp followed by wash-out, under basal conditions and after LTP-induction. Jasp treatment seem to interfere with LTP-induced nanoscale organization of PSD95.

Conclusion & Discussion

Scaffolding proteins, such as PSD95 and the Shank protein family, are responsible for positioning AMPARs within the PSD (Bats *et al.,* 2007; Schnell *et al.,* 2002; Naisbitt *et al.,* 1999). The positioning of AMPARs relative to presynaptic sites of neurotransmitter release influences synaptic strength (Boucher *et al.,* 2010; Raghavachari & Lisman, 2004; Franks *et al.,* 2003). Previous studies showed that PSD scaffolding proteins are organized into nanodomains aligned to presynaptic release sites (MacGillavry *et al.,* 2013; Nair, et al., 2013; Broadhead et al., 2016; Tang *et al.,* 2016; Fukata *et al.,* 2013). The organization of these nanodomains within the PSD changes during synaptic plasticity (Wiesner *et al.,* 2020; Hruska *et al.,* 2018; Serweta *et al.,* 2021 unpublished). Furthermore, the presence of Shank3 was shown to be vital for LTP-induced reorganization of PSD95 (Serweta *et al.,* 2021 unpublished). However, it is still unknown which specific molecular interactions are involved in organizing the subsynaptic PSD95 distribution, maintaining this distribution and regulating PSD95 reorganization during synaptic plasticity.

It is possible that Shank3 regulates PSD95 organization through its interaction with scaffolding protein GKAP. The Shank3 PDZ-domain, together with two flanking sequences called the β-hairpin and the BC-loop, can bind to the C-terminal domain of GKAP (Naisbitt *et al.,* 1999; Zeng *et al.,* 2016).

In turn, GKAP binds via its N-terminus to PSD95, which interacts with the AMPARs and their auxiliary subunits through its PDZ domain (Bats *et al.,* 2007; Schnell *et al.,* 2002). The interaction between Shank3 and GKAP therefore couples Shank3 to the upper layers of the PSD and ultimately, the AMPARs. Using super-resolution dSTORM imaging, we found that weakening the binding between Shank3 and the upper PSD through its connection with GKAP, leads to an LTP-like reorganization of PSD95. In addition, Shank3 interacts with the actin cytoskeleton, a structure that is essential for lasting LTP (Nakahata & Yasuda, 2018; Okamoto *et al.,* 2004 ; Kim & Lisman, 1999; Krucker *et al.,* 2000) and could be involved in regulating the PSD nanostructure. We disrupted the interaction of Shank3 with F-actin itself and with two actin-interacting proteins (cortactin and ABI1). This was done to determine which specific Shank3-actin interactions could be involved in regulating PSD95 organization. However, none of these disruptions led to a significant change in PSD95 organization under basal conditions. Nevertheless, the actin cytoskeleton does seem to play a role in regulating the subsynaptic PSD95 distribution. It was found that depolymerizing the actin cytoskeleton through treatment with LatB leads to a delayed increase in the number of PSD95 nanodomains. Furthermore, disrupting the actin cytoskeleton with either LatB or Jasp might impair LTP-associated PSD95 reorganization. These results point to an important role for both Shank3 and the actin cytoskeleton in maintaining PSD95 organization.

The connection between Shank3 and the upper layers of the PSD could be important for stabilization of the PSD95 nanoscale distribution

To determine whether the direct interaction between Shank3 and PSD95 through GKAP is involved in regulating the PSD95 organization, this interaction was weakened through deletion of the Shank3 β-hairpin sequence. Surprisingly, dSTORM imaging showed that decoupling Shank3 from the upper PSD induces an LTP-like increase in PSD95 nanodomain number and density (Fig.2B,C,D). These results indicate that Shank3 may not actively drive PSD95 reorganization, but instead could be involved in maintaining PSD95 organization under basal conditions. Releasing the upper PSD from the direct influence of Shank3 is enough to allow for PSD95 reorganization.

However, if it is purely the direct interaction between GKAP and Shank3 that governs PSD95 nanoscale (re-)organization, the effects of completely removing Shank3 on the PSD organization should be similar to the effects of decoupling Shank3 from GKAP. It is therefore interesting that previous studies showed that knocking down Shank1-3 does not lead to an increase in nanodomain number and density during synaptic plasticity, but instead abolishes LTP-associated PSD95 reorganization (Serweta *et al.,* 2021, unpublished). This could mean that uncoupling Shank3 from the upper PSD has a different effect on PSD95 nanoscale organization than completely removing it from the PSD. Alternatively, the effects of both removing and uncoupling Shank3 could be plasticity dependent. For example, both removing Shank3 and decoupling it from the rest of the PSD could cause an aberrant PSD95 distribution in the PSD. Since these PSDs are already free from any control exerted by Shank3, LTP might not induce any additional PSD95 reorganization. It is therefore important to determine if LTP induction still causes PSD95 reorganization in neurons re-expressing Shank3 Δβ-hairpin. Unfortunately, our attempts at inducing LTP within Shank3r Δβ-hairpin expressing neurons seemed unsuccessful. LTP induction did not lead to the characteristic PSD95 reorganization for neurons re-expressing Shank3r WT (Supplementary Fig. 4A,B). This could be due to mistakes during LTP induction. Alternatively, it is possible that the control medium that was used for the control condition and for recovery has an effect on PSD95 organization that masks or impedes LTP-induced PSD95 reorganization.

Nevertheless, even if the Δβ-hairpin mutation abolishes LTP-induced PSD95 reorganization, previous experiments did not seem to show an LTP-like increase in PSD95 nanodomain number and density after Shank1-3 depletion under basal conditions (Serweta *et al.,* 2012 unpublished). This indicates that Shank3 might have an additional role in PSD95 reorganization, besides its direct influence on the PSD. An alternative explanation could therefore be that the weakening of the interaction between the upper PSD and Shank3 causes the activation of other molecular pathways that involve Shank3. Shank3 interacts with many important signalling molecules such as small GTPases Rho, Ras and Rap (Salooma *et al.,* 2020; Lilja *et al.,* 2017). It was also shown that Shank3 can influence transsynaptic signalling through neurexins and neuroligins (Magali *et al.,* 2012). On top of that, Shank3 is phosphorylated by and interacts with CAMKIIα (Jeong *et al.,* 2021; Perfitt *et al.,* 2020), a kinase that is known to be vital for LTP-induction (reviewed by Lisman *et al.,* 2012). It is possible that releasing the control exerted on the PSD by Shank3 leads to the recruitment or activation of these other signalling molecules and proteins. These molecules could then start signalling cascades that further stimulate PSD95 reorganization. However, this is all highly speculative and would have to be confirmed by further experiments in which the interactions between Shank3 and these specific molecules are disrupted. For now, it can only be concluded that weakening the link between PSD95 and Shank3 through GKAP, allows for PSD95 reorganization.

Disrupting a single interaction between Shank3 and actin or actin binding proteins does not significantly influence PSD95 nanoscale organization

It is known that actin dynamics are increased during plasticity and that blocking actin dynamics abolishes LTP (Nakahata & Yasuda, 2018; Okamoto *et al.,* 2004 ; Kim & Lisman, 1999; Krucker *et al.,* 2000). It is therefore possible that the actin network influences PSD95 organization through Shank3. Three Shank3 mutants were created that block or weaken Shank3-actin interactions. The Q37A/R38A mutation disrupts the direct binding of Shank3 to F-actin (Salooma *et al.,* 2020). The S685I and ΔPro mutations disturb the interaction with actin nucleation promoting factors ABI1 and cortactin, respectively (MacGillavry *et al.,* 2016; Wang *et al,* 2020). Neither disrupting the direct binding between Shank3 and actin, nor the interaction with ABI1 or cortactin led to any discernible changes in subsynaptic PSD95 organization (Fig.4A-F). However, this does not necessarily mean that these interactions are not involved in regulating PSD95 organization. Shank3 interacts with many different actin interacting proteins besides cortactin, ABI1 and its direct interaction with actin. It is therefore possible that the relative contributions of each individual interaction are too small to detect. Alternatively, there could be redundancy between these interactions. For example, both cortactin and ABI1 are actin nucleation promoting factors that function through activation of the Arp2/3 complex. It is therefore possible that they could compensate for each other's absence. Another possibility is that some of these interactions are not important for the maintenance of the subsynaptic organization of PSD95 under basal conditions. However, they could still be involved in LTP-associated PSD95 reorganization. During LTP the actin network undergoes extensive remodelling (Okamoto *et al.,* 2004). Recruitment and activation of actin nucleating factors, actin polymerizing factors and actin depolymerizing factors by Shank3 could therefore play an important role in inducing LTP-associated actin dynamics. Unfortunately, our results for the effects of the Q37A/R38A, ΔPro and S685I mutations on LTP-induced PSD95 reorganization were inconclusive. Similar problems presented as for the Δβ-hairpin mutation. LTP-induction did not lead to PSD95 reorganization in the control neurons expressing the Shank3r WT construct (Supplementary Fig.5).

Depolymerizing the actin network might allow PSD95 reorganization

Interfering with the interactions between Shank3 and F-actin, cortactin and ABI1 did not influence PSD95 nanoscale organization. Nevertheless, actin dynamics do seem to be involved in regulating the subsynaptic PSD95 distribution. Promoting actin depolymerization by treatment with LatB led to a delayed increase in the number of nanodomains (Fig.3B). It is possible that actin depolymerization causes the decoupling of the actin cytoskeleton from the PSD. This could point to a model in which the actin cytoskeleton inhibits PSD reorganization under basal conditions. The control of the actin cytoskeleton could be transferred to the PSD through Shank3. When the influence of the actin cytoskeleton on the PSD is removed, the PSD could become free to reorganize. This would mean that the connection of the actin cytoskeleton and Shank3 to the upper PSD is not the driving force behind PSD95 reorganization, but rather the force that maintains PSD95 organization.

Additionally, both LatB and Jasp treatment plus wash-out seem to impair LTP-associated reorganization of PSD95 (Fig.6B,C). LatB causes actin depolymerization, which could release the PSD from the actin cytoskeleton and lead to an increase in the number of nanodomains. LTP induction might therefore no longer be able to cause any additional reorganizations. In the case of Jasp, other mechanisms might be at play. Jasp stabilizes the actin network. This could prevent the necessary breakdown of the actin network that is needed to release its control on the PSD, which in turn impedes PSD95 reorganization. However, it is currently unknown what the exact effects of Jasp and LatB wash-out are on actin dynamics. Therefore, the live-cell imaging experiments (Supplementary Fig.6) that were set-up during this study need to be continued in order to gain a better understanding of what happens after Jasp and LatB wash-out.

A hypothetical model for LTP-induced PSD reorganization

Releasing the PSD from the spine actin cytoskeleton, either through depolymerization of the actin network or by decoupling Shank3 from the upper PSD, leads to an LTP-like PSD95 reorganization. Based on these results, a hypothetical model for PSD95 reorganization during LTP can be construed (Fig.7). During the initial phases of LTP, actin stabilizing factors are removed from the PSD, while actin severing factors are recruited (Bosch *et al.,* 2014; Mizui *et al.,* 2014). Filament severing causes F-actin to become shorter and leads to a net breakdown of the actin cytoskeleton (Chen *et al.,* 2015). This breakdown could lead to a release of the influence that the actin network normally exerts on the PSD through Shank3. This release allows for PSD95 reorganization. During PSD95 reorganization, actin polymerizing and branching factors stimulate rebuilding of the actin cytoskeleton. After PSD95 reorganization is complete, the remodeled actin cytoskeleton could stabilize and consolidate the new PSD organization, resulting in lasting LTP. If this model is correct, it gives us exciting new insights into synaptic functioning. However, in order to determine validity of this tentative model, additional research is necessary.

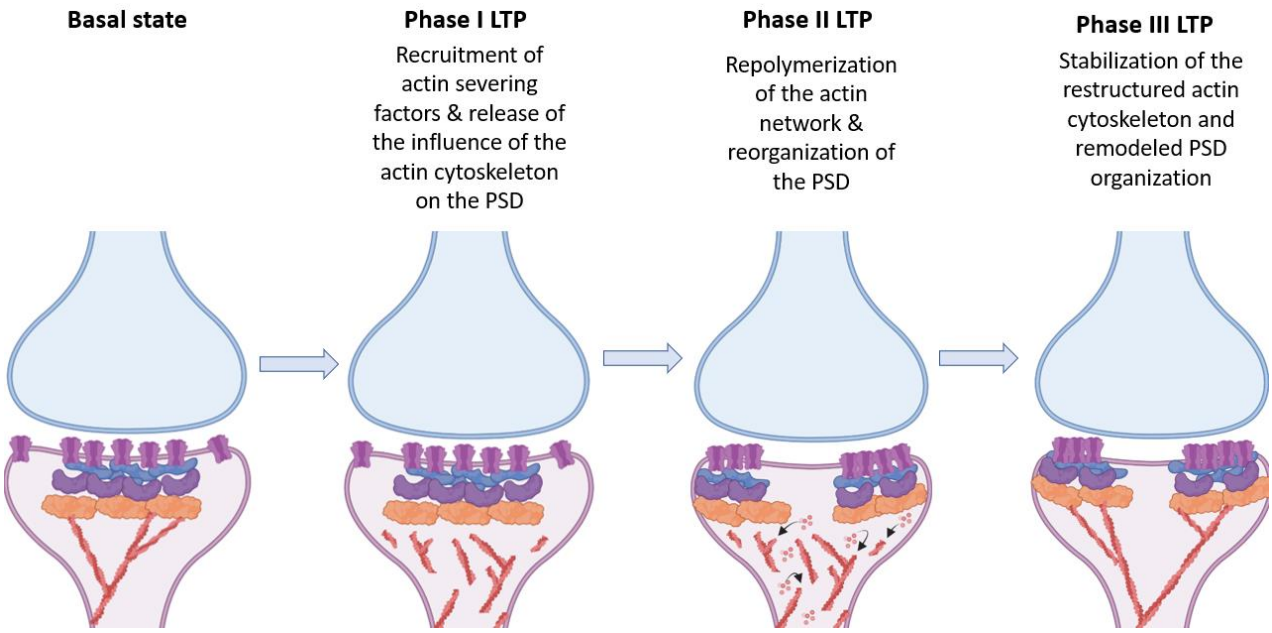

Figure 7. Hypothetical model for PSD reorganization during LTP. Directly after LTP-induction, actin stabilizing proteins leave the spine, while F-actin severing proteins are recruited. This leads to a net breakdown of the actin network. As a result of the breakdown, the actin cytoskeleton no longer exerts its control on the upper PSD through Shank3. The PSD starts to reorganize. Finally, the actin cytoskeleton is remodelled and rebuild and stabilizes the changed PSD nanostructure, ensuring lasting expression of LTP.

Future perspective

This study hypothesizes that the actin cytoskeleton maintains the PSD nanoscale organization through its interaction with Shank3. Releasing the PSD from the constraints imposed by the actin cytoskeleton could allow for reorganization of the PSD during synaptic plasticity. This hypothesis raises many new exciting questions that need to be answered.

Firstly, the effect of different types of actin dynamics on the PSD nanoscale organization need to be determined. This could be done by combining live-cell imaging with the treatment of LatB and Jasp or other drugs that disrupt actin in neurons. Subsequently, neurons should undergo the same drug-treatment, be fixated and imaged using dSTORM to determine any effects that these drugs have on PSD nano-organization. Then, changes in PSD95 nanoscale organization can be correlated to changes in actin dynamics. Additionally, the relative importance of specific Shank3/actin interactions for regulating the PSD95 nanoscale organization needs to be elucidated. Double or triple Shank3 re-expression mutants can be created to simultaneously disrupt interactions that could be redundant. On top of that, the effects of these mutations on LTP-induced PSD95 nanoscale reorganization should be determined. In this way, interactions that are specifically involved in LTP-associated PSD95 reorganization can be identified. Additionally, the reorganization of other scaffolding proteins that form nanodomains can be examined. It is important to compare the reorganization of different PSD scaffolding proteins and AMPARs over time in order to determine the sequence of events that takes place during reorganization and to determine whether it is likely that the reorganization of all these molecules is driven by the same processes. On top of that, changes in the postsynaptic PSD organization should be correlated to changes in the presynaptic organization in the active zone.

Another crucial step that needs to be taken is to correlate different PSD95 nanoscale organizations to synaptic functioning using electrophysiology. First, it needs to be determined if abolishing LTP-induced PSD reorganization affects lasting strengthening of the synapse. This could be done through knockdown of Shank1-3 in a rat hippocampal neuron culture, followed by chemical LTP induction to potentiate a large proportion of synapses in the culture (Molnar, 2011). After LTP induction, both spontaneous (miniature EPSPs) and evoked (EPSPs) transmission in these cells can be measured through patch-clamp experiments (Hill & Stephens, 2021). Subsequently, the effects of different Shank3 mutations on synaptic functioning should be determined in a similar fashion. First, the effects of the mutation on basal transmission (spontaneous and evoked) can be determined with electrophysiology. Then, the capacity of the Shank3 mutant neurons for lasting LTP should be tested.

Ultimately, changes in the PSD nanoscale organization and their influence on synaptic transmission need to be translated to the functioning of the brain and the organism as a whole. After the effects of a specific mutation on the PSD nanoscale organization and synaptic functioning have been determined in neuronal cultures, this mutation can be introduced into rats or mice. Using CRISPR/Cas9 the mutation can be introduced in rat or mice zygotes (Qin *et al.,* 2015). For deletion mutations, such as the deletion of specific Shank3 domains, it might even be possible to create conditional mutant rats or mice that only express the mutation in specific tissues, such as the hippocampus. This can be achieved by generating a mouse line in which the sequence that has to be deleted is floxed (flanked by loxP sites). The floxed version of the target gene is introduced into mouse or rat zygotes using CRISPR/Cas9 (Quadros *et al.,* 2017). The resulting floxed mouse or rat line can then be cross bred with another transgenic mouse or rat line that expresses a Cre-recombinase under a tissue-specific promotor (Gierut *et al.,* 2014; Quadros *et al.,* 2017). These mutant mice or rats could be used for the harvest of acute brain slices. Subsequently, these slices can be used for electrophysiological recordings to confirm the results that were obtained in neuronal cultures. Subsequently, the capacity for learning and memory formation in the mutant rats can be investigated using various tests, such as the Morris Water maze (Bromley-Brits *et al.,* 2011) and compared to wildtype rats. By characterizing the effects of a wide array of PSD protein mutations on the learning capability of animals, it might be possible to determine if mutations that have a similar effect on PSD organization and synaptic functioning also lead to similar behavioural phenotypes. Furthermore, it is known that many neuronal disorders, such as Autism Spectrum Disorders, are associated with mutations in Shank3 and defects in synaptic signalling (Wilson *et al.,* 2003; Durand *et al.,* 2007; Bozdagi *et al.,* 2010; Kouser *et al.,* 2013). Therefore, the rat behavioural tests could be expanded to include tests for autism symptoms, such as tests for social behaviour and grooming. By doing this, our knowledge about the molecular pathways that are involved in learning and in the development of neuronal disorders, could be increased.

This study has set the next step towards identification of the molecular mechanisms driving PSD nanoscale (re-)organization and its relevance for synaptic functioning. Further progression on this topic, will help us gain understanding of learning and memory processes. This will not only give us new insights into the normal functioning of the brain, but eventually also lead to new opportunities for understanding, preventing and treating synaptopathic neuronal disorders.

Materials and methods

Primary rat neuronal cultures

The use of all rats required for experiments was approved by the Dutch Animal Experiments Committee (Dier Experimenten Commissie [DEC]). All animals were cared for in accordance with the regulations of Utrecht University, Dutch law (Wet op de Dierproeven, 1996) and European regulations (Directive 2010/64/EU).

Dissociated hippocampal cultures were prepared from both female and male embryonic day 18 (E18) Wistar rats. The neurons were plated in a 12-wells plate at an average density of 100,000 neurons per well on 18 millimetre-wide glass coverslips (type 1) with a coating of laminin (1.25 mg/ml, Roche Diagnostics) and poly-L-lysine (37.5 mg/ml, 818 Sigma-Aldrich). During maturation (day in vitro 1-7 [DIV1-7]), neurons were kept at 37 °C and 5% CO_2 in Neurobasal Medium (NB; Gibco) supplemented with 2% B27 (Gibco), 0.5 mM glutamine (Gibco), 15.6 µM glutamate (Sigma) and 1% Penicillin/Streptomycin (P/S, Gibco). After DIV7, the neurons underwent weekly replacement of 50% of the medium by BrainPhys neuronal medium (BP, STEMCELL Technologies) with added 2% NeuroCult SM1 (STEMCELL Technologies) and 1% P/S (Gibco).

DNA constructs

A PSD95-HaloTag knock-in construct that was previously created by our lab, was used to label endogenous PSD95 to determine its subsynaptic distribution using dSTORM. The construct was created using the CRISPR/Cas9 based ORANGE toolbox (Willems *et al.,* 2020). Additionally, a previously created ORANGE β-actin knock-in construct was used that labels endogenous F-actin and G-actin with a Halo-Tag, to determine the effects of LatB and Jasp treatment and wash-out on the actin network. A Homer1c-ALFA overexpression construct was used as a PSD-marker for the validation of the Shank3r mutants.

The Shank3r mutant constructs were used to determine the role of specific Shank3 mutations in regulating PSD95 nanoscale distribution. Shank1-3 miRNA based knockdown construct (pSM155 mirShank-mCherry) and the Shank3 wildtype re-expression construct (pSM155 mirShank::mCherry-Shank3) were previously characterized in MacGillavry *et al.* (2016) and Scheefhals *et al.* (2019) respectively. The Shank3 mutations (Shank3 S685I, Shank3 Δβ-hairpin, Shank3 ΔPro, Shank3 Q37A/R38A) were introduced into the Shank3 re-expression construct using In Vivo Assembly cloning (IVA cloning; García-Nafría *et al.,* 2016). First, forward and reverse primers were designed for the PCR amplification of each mutation (Table 1). These primers consist of a template binding region that binds the Shank3 re-expression construct at the site that is to be mutated and a short homologous flanking sequence. The homologous regions were at least 15 base pairs (bp) long with a melting temperature of 48-52 °C. The melting temperature for the template binding regions of the primer was approximately 60 °C. Shank3 point mutations were introduced at the 5'end of the forward primer in between the homologous flanking region and the template binding region. Shank3 deletions were introduced by creating primers that bind on one side each, outside of the sequence that is to be deleted. After primer design, the constructs were created using a single-step PCR reaction followed by Dpn1 digestion and transformation of DH5α bacteria. The PCR reaction mixture contained 10 µM of each of the primers, 20 ng template DNA, 0.25 µL Phusion DNA polymerase, 5 µL 5x Phusion buffer, 0.5 µL 10 µM deoxynucleotide triphosphate (dNTPs), 1.5 µL DMSO and 17.25 µL

MilliQ water. The PCR protocol consisted of 18 cycles of 10 seconds at 95 °C, 30 seconds at 60 °C and 4 minutes at 72 °C. After PCR amplification, 1 µL of the Dpn1 endonuclease for methylated DNA was added to digest the original template DNA. Then, 50 µL DH5α bacteria were transformed with 5 µL of the digestion mix. After addition of the DNA, bacteria were placed on ice for 30 minutes, heat-shocked for 45 seconds at 42 °C and placed back on ice for 5 minutes. Then, 200 µL of LB was added and the bacteria were incubated at 37 °C for 30 minutes, to allow them to express the kanamycin resistance gene present in the DNA construct. Afterwards, the bacteria were plated on an LB plate with kanamycin. The bacteria were incubated at 37 °C overnight.

Tabel 1: PCR primers for IVA cloning of the Shank3 mutations

#	Mutation/deletion	Forward primer (5'-3')	Reverse primer (5'-3')
1	Shank3 Δβ-hairpin	ACAAGAGAGGACCGGGTGATCGACGATAAGGTGGCCGT	CCGGTCCTCTCTTGTCTCGG
2	Shank3 Q37A/R38A	TGTGGGCCGCCAAAGCGGCGGTGCTGTGCGCTCTGAACCAC	TTTGGCGGCCCACACAGGAG
3	Shank3 ΔPro	ACCTTTCTGCTGGAAAAGCTGAAGTCCCCTCTGGG	TTCCAGCAGAAAGGTATGGCCG
4	Shank3 S585I	CCTAAGAGAGCCCCTATCACCACCCTGACCCTGCG	AGGGGCTCTCTTAGGGGGT

Transfection

Cultured rat hippocampal neurons were transfected at DIV4 using Lipofectamine 2000 reagent (Invitrogen). Prior to transfection, 500 µL medium from each well was transferred to a new 12 wells plate. The medium in the new 12 wells plate was mixed with an additional 500 µL NB supplemented with 2% B27, 0.5 mM Glutamine, 15.6 µM glutamate and 1% Pen/Strep. 300 µL pre-warmed NB with 0.5 mM L-glutamine was added to the old plate, immediately followed by 200 µL DNA mixture containing NB, 3.3 µL Lipofectamine 2000 and DNA per well. To identify aberrations in synaptogenesis, Shank3 localization and synaptic enrichment caused by the introduction of mutations in the Shank3r construct, neurons were transfected with the Shank3r WT or mutant (Δβ-hairpin, Q37A/R38A, ΔPro, S685I) construct and a Homer1c-ALFA overexpression construct. For determining the effect of specific Shank3 mutations on PSD95 nanoscale organization, the neurons were transfected with the pORANGE Dlg4-HaloTag knock-in construct and the Shank3r WT or mutant (Δβ-hairpin, Q37A/R38A, ΔPro, S685I). To determine the effects of LatB and Jasp on the PSD95 nanoscale organization, the cells were transfected with pORANGE Dlg4-HaloTag. Lastly, to observe the effects of LatB and Jasp treatment plus wash-out on the dynamics of the actin network, the neurons were transfected with the pORANGE β-actin-HaloTag knock-in construct.
Neurons were incubated with the DNA mixture for 90 minutes and were subsequently washed in pre-warmed NB, transferred to the new 12 wells plate and kept at 37 °C and 5% CO_2 until further experiments at DIV20-23.

Chemical LTP induction

To induce Long-Term Potentiation, a chemical LTP (cLTP) induction protocol was used. This protocol causes the activation of the NMDA receptor, which leads to an influx of Ca^{2+} ions into the postsynaptic cell, resulting in LTP (Lynch *et al.,* 1983; MacDermott *et al.,* 1986; Regehr & Tank, 1990). The medium for LTP induction contained 260 µM glycine, 25 µM bicucullin, 140 mM NaCl, 3 mM KCl, 10 mM HEPES, 2.67 mM $CaCl^2$, 10 mM glucose and 25.7 mM sucrose. For the control condition, control medium was used instead. The control medium contained 140 mM NaCl, 3 mM KCl, 10 mM HEPES, 2.67 mM $CaCl^2$, 10 mM glucose, 4.29 mM $MgCl_2$ and 15.2 mM sucrose.
The osmolarity (305-320 mOsm) and pH (7.3-7.4) of both media matches that of the culture medium (BP) the neurons are kept in prior to LTP induction, to prevent osmotic shock. 300 µL control or cLTP medium was added to the wells of a 12-wells plate and pre-warmed at 37 °C. For the experiments

using LatB and Jasp, 1 µM LatB (Tocris Bioscience), 0.2 µM Jasp (Tocris Bioscience) or 0.2 µL DMSO was added to the control and cLTP medium. Before cLTP induction, the cells were live-cell labelled with Halo-Ligand JF646 (200 nM, Promega). The neurons were incubated in 50 µL Halo-Ligand solution for 10 minutes at 37 °C and 5% CO_2. Afterwards, they were returned to their original 12-wells plate and kept at 37 °C and 5% CO_2 for 15-60 minutes. Then, to start cLTP induction, the coverslips were dipped in either control or cLTP medium and transferred to the pre-warmed 12 wells plate containing control or cLTP medium. They were kept at 37 °C for 5 minutes. After 5 minutes, the cells were either fixated for the 5-minute condition or the medium was replaced with 500 µL control medium and placed back at 37 °C for 55 minutes. After 55 minutes, the remaining cells were also fixated at 37 °C for 5 minutes in 500 µL 4% EM-grade paraformaldehyde (PFA, Electron Microscopy Science) in PEM80 buffer (80 nM PIPES, 1 mM EGTA, 2 mM $MgCl_2$, pH=6.9). Coverslips were washed 3 times for 10 minutes with 1 mL PBS/glycine (0.1 M glycine). Finally, the neurons were kept in 1 mL PBS/glycine until imaging.

Nanobody staining

The effect of the Shank3 mutations (Δβ-hairpin, Q37A/R38A, ΔPro, S685I) on synaptogenesis and Shank3 localization and synaptic targeting was investigated. After fixation and cLTP induction on DIV21-23, the cultured rat hippocampal neurons that were transfected with the Shank3r WT and mutant (Δβ-hairpin, Q37A/R38A, ΔPro and S685I) constructs and the Homer1c-ALFA construct were stained for Homer1c-ALFA. Prior to staining, the sample was blocked using blocking buffer that contained 10% v/v normal goat serum (NGS) and 0.1% Triton X-100 in PBS/glycine. The neurons were incubated in 300 µL blocking buffer for 30 minutes at 37 °C. After blocking, the neurons were incubated with the nanobody mixture. This mixture is a 1:500 dilution of the anti-ALFA Atto488 nanobody (NanoTag) in 5% v/v NGS, 0.1% v/v Triton X-100 in PBS/glycine. The coverslips were placed with their cells down on 50 µL droplets of nanobody mixture for 90 minutes at room temperature. After 90 minutes, the coverslips were washed 3x10 minutes with 1 mL PBS/glycine. Finally, the neurons were washed a fourth time with 1 mL Milli-Q. Then, the coverslips were mounted onto glass slides with 12 µL Polyvinil alcohol mounting medium with DABCO (Sigma Aldrich).

Laser-scanning confocal microscopy

After transfection with Shank3r WT or one of the Shank3r mutants (Δβ-hairpin, Q37A/R38A, ΔPro and S685I) and Homer1c-ALFA, the neurons were stained for Homer1c-ALFA. Then, they were imaged with the Carl Zeiss LSM700 laser-scanning confocal microscope. The microscope uses ZEN 2011 software and has 4 laser lines: 405 nm, 488 nm, 555 nm and 633 nm. For imaging, the Plan-Apochromat 63x/1.40 Oil immersion objective and the 488 and 555 nm lasers were used. The number of pixels for each image was 2024x2024. Images were acquired as z-stacks with a 0.5 µm interval between each imaging slice. After imaging, the images were further processed in ImageJ. Intensity projections were created and PSDs were identified based on the Homer1c signal using the ComDet Plug-in (Katrukha, 2021). The intensity threshold for identification of Homer1c punctae was set to 12 and for Shank3r punctae to 2.50. To determine the colocalization between the Homer1c and Shank3 signal with the ComDet plug-in, a maximum distance of 4 pixels between colocalized spots was chosen. Additionally, the fluorescence intensity in the dendritic shaft and PSDs of three dendrites per neuron (2 PSDs/dendrite) was determined using the measure function of ImageJ. The background intensity was subtracted from the measured shaft and PSD fluorescence intensity for both the Shank3 and Homer1c signal. These values were used to calculate the PSD/Shaft intensity ratio for the Shank3 and Homer1c signal.

Stochastic Optical Reconstruction Microscopy and Data processing

Stochastic Optical Reconstruction Microscopy (dSTORM) was used for super resolution imaging of endogenously labelled PSD95 in fixated neurons, either under basal conditions or after cLTP induction. This method was used to observe changes in the PSD95 nanoscale distribution in response to different Shank3 mutations and to treatment with LatB and Jasp. Before imaging, the coverslips were mounted onto a glass slide in a solution with 30 µM MEA, 700 µg/ml glucose oxidase and 5% glucose in 1x PBS. All dSTORM data was acquired with the Nanoimager S microscope (Oxford Nanoimaging Ltd.). The Nanoimager S has a XYZ closed-loop piezo stage, a 100x oil immersion objective and four lasers: 405 nm, 471 nm, 561 nm and 640 nm. Fluorescent signals emitted from the sample were detected with a sCMOS camera (ORCA Flash 4, Hamamatsu). For acquisition of widefield images, samples were illuminated with the 640 nm laser for 50 frames at 50 Hz. For acquisition of dSTORM images, samples were illuminated with the 640 nm laser with oblique illumination (angle 53 °) for 15,000 frames at 50 Hz. During acquisition the intensity of the 405 nm laser was steadily increased to keep stochastic blinking of Janelia Fluor 646 optimal. After acquisition, dSTORM reconstruction and drift correction were performed using the NimOS software, followed by further drift correction with the Detection of Molecules (DoM) plugin v.1.2.1 for ImageJ (Katrukha, 2020). Further data analysis was performed in MATLAB (2020).

Only molecules with more than 300 photons and a localization precision of less than 15 nm were included in the analysis. Subsequently, recurrent localizations that were present in more than one frame, were filtered out by tracking (tracking radius of 60 nm). A maximum-intensity projection of a 50-frame wide-field stack image of the PSD95-HaloTag signal was used to define the Regions Of Interest (ROIs), which in this case are the PSDs. Next, PSD95 nanodomains were identified with the DBSCAN algorithm in MATLAB (Ester *et al.,* 1996). For nanodomain identification, clusters were selected that contained more than 800 localizations and were between 0.01 μm^2 and 0.3 μm^2 in size. The local density represents the number of localizations within a radius of 5 times the mean nearest neighbor distance of all molecules in the nanodomain. Localizations were considered to be inside a nanodomain if their local density was higher than 40. The MATLAB functions linkage() and cluster() were used to isolate individual nanodomains. When the local density peaks of two possible nanodomains were further apart than 80 nm and were separated by a local minimum of less than 30% of the maximal local density, the clusters were counted as two separate nanodomains. Nanodomains that contained less than 5 localizations or had a diameter of less than 30 nm were excluded. Within PSDs, molecules were plotted and color-coded according to the local density (MacGillavry *et al.,* 2013).

Spinning disk live cell imaging

To observe what happens to the dynamics of the actin network after 5 minutes of treatment with LatB or Jasp followed by 55 minutes of wash-out, the neurons were live-cell imaged. Prior to imaging, the neurons were live-cell labelled with Halo-Ligand JF549 (200 nM, Promega). The neurons were incubated in 50 µL Halo-Ligand solution for 10 minutes at 37 °C and 5% CO_2. Afterwards, they were returned to their original 12-wells plate and kept at 37 °C and 5% CO_2 for 15-190 minutes. After labelling, the neurons were mounted onto Ludin chambers in 500 µL pre-warmed control medium. Then, the cells were imaged with the Nikon Eclipse Ti2 confocal spinning disk microscope. The microscope contains five laser lines: 405 nm, 446 nm, 488 nm, 561 nm and 642 nm. For live-cell imaging of endogenously labelled β-actin, the Plan-Apochromat 100x/1.45 OIL immersion objective and the 561 nm laser were used. To be able to acquire z-stacks of multiple cells over time, the Multi Dimensional Acquisition mode (MetaMorph)

was used. The neurons were imaged 16 times over a duration of 75 minutes, meaning an acquisition was taken every 5 minutes. The 561 nm laser was used with the gain set to 3 and the exposure set to 500 ms. For the Z-series the interval was set to 0.5 µm with a total stack volume of 5 µm. 15 minutes after the start of imaging, the control medium in the Ludin chamber was exchanged with treatment medium, which is 500 µL control medium with 2 µL DMSO, 500 µL E5 with 1 µM LatB or 500 µL E5 with 0.2 µM Jasp. The neurons were left in the treatment medium for 5 minutes, after which the medium was again exchanged twice for 500 µL control medium. After treatment, imaging was resumed for another 55 minutes. The acquisitions were further processed in ImageJ. First, maximum intensity projections were created. Then, drift was corrected using the TurboReg and StackReg Plug-ins. The background was subtracted using a rolling ball radius of 3.15 µm. Then, the PSDs in each neuron were identified with the ComDet Plug-In (Katrukha, 2021). The frame in which the most PSDs were identified was chosen and the ROIs were saved in the ROI manager. Integrated densities (InDen) were determined for each frame. Subsequently, a macro developed by Jacob Prues was used to subtract each frame (t_x) from the previous frame (t_{x-1}). After application of the macro, the InDen was measured again. Finally, a frame-to-frame correlation was obtained using the formula: $(\text{InDen } t_x - [\text{InDen } t_x - \text{InDen } t_{x-1}])/\text{InDen } t_x$. The frame-to-frame correlation was plotted over time. Unfortunately, not enough data could be collected to draw any conclusions from the live-cell data.

Statistical analyses

All statistical analyses were performed in GraphPad PRISM (versions 9 and 8). If the data was normally distributed and equally dispersed, an unpaired t-test was used to compare 2 groups with each other. Alternatively, one-way ANOVA was performed to compare 3 or more groups with each other. Afterwards Sidak's multiple comparisons test was used to do post-hoc multiple comparisons. For all experiments, a minimum of 8 cells per timepoint and experimental condition were included. All data was displayed in bar graphs with the mean +/- the standard error of the mean (SEM).

Supplementary figures

Shank3 Δβ-hairpin, Q37A/R38A, ΔPro and S685I mutations do not impair Shank3 synaptic targeting or synaptogenesis

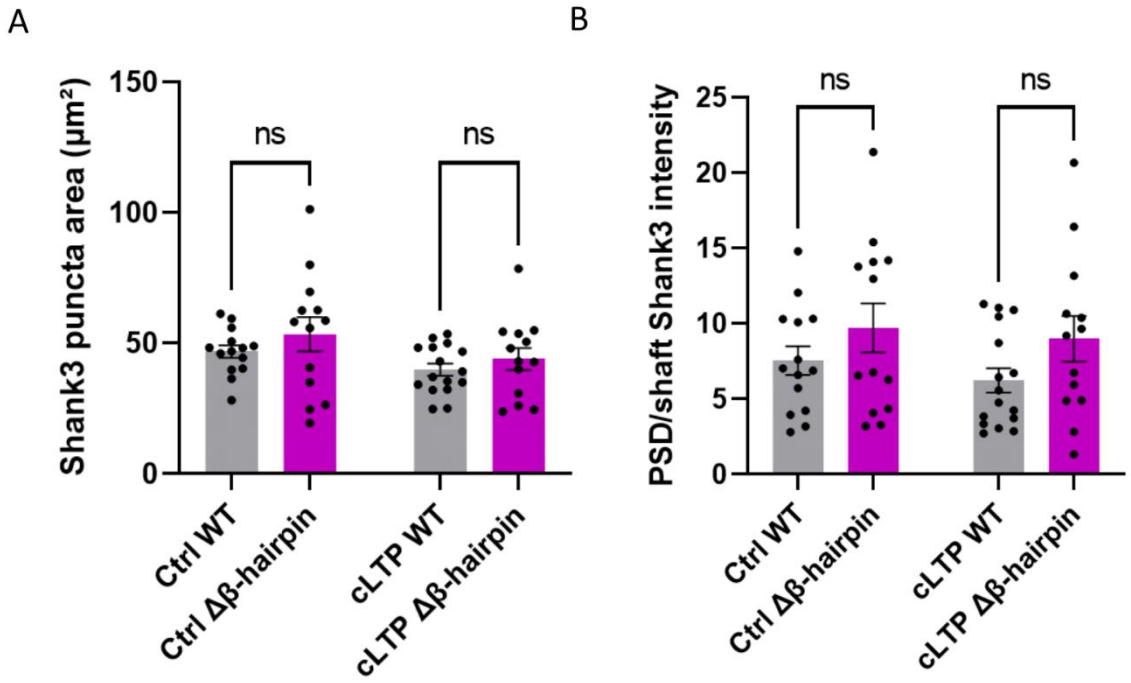

Supplementary figure 1. The Shank3 Δβ-hairpin mutation does not influence Shank3 synaptic targeting.

A. Mean area of Shank3 punctae in the PSDs of neurons transfected with Shank1-3 KD + Shank3r WT or Shank3r Δβ-hairpin and Homer1c-ALFA. No differences were found between Shank3r WT and Shank3r Δβ-hairpin area under basal conditions (WT=46.77 +/- 2.47 µm^2; n=14; Δβ-hairpin=53.48 +/- 6.56 µm^2; n=13; ANOVA; Sidak's multiple comparisons test; p=0.44) or LTP (WT=39.84 +/- 2.32 µm^2; n=16; Δβ-hairpin=43.96 +/- 4.29 µm^2; n=13; ANOVA; Sidak's multiple comparisons test; p=0.71).

B. Ratio of the mCherry-Shank3 fluorescence intensity in the PSD: mCherry -Shank3 fluorescence intensity in the dendritic shaft. No significant differences were found between Shank3 WT and Shank3 Δβ-hairpin under basal conditions (WT=7.54 +/- 0.95; n=14; Δβ-hairpin= 9.72 +/- 1.62; n=13; ANOVA; Sidak's multiple comparisons test; p=0.40) or after LTP (WT=6.23 +/- 0.81; n=16; Δβ-hairpin=8.94 +/- 1.52; n=13; ANOVA; Sidak's multiple comparisons test ; p=0.21).

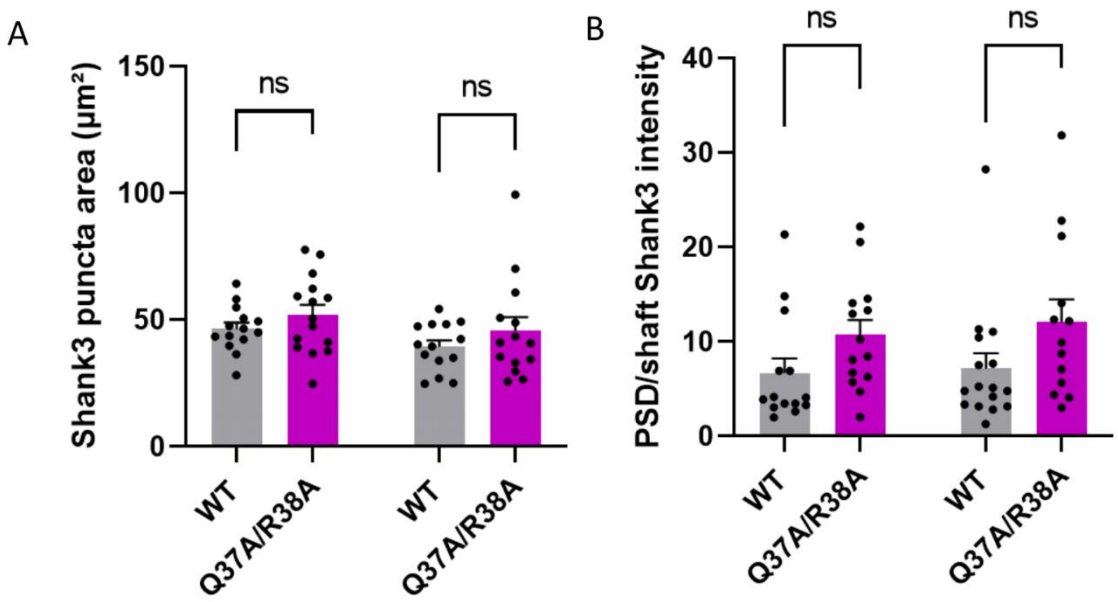

Supplementary figure 2. Shank3 Q37A/R38A does not influence Shank3 synaptic targeting.

A. Mean area of Shank3 punctae in the PSDs of neurons transfected with Shank1-3 KD + mCherry-Shank3 WT or Shank1-3 KD + mCherry-Shank3 Q37A/R38A and Homer1c-ALFA. No differences were found between Shank3 WT and Shank3 Q37A/R38A area under basal conditions (WT=46.48 +/- 2.43 μm^2; n=14; Q37A/R38A=51.98 +/- 3.95 μm^2; n=15; ANOVA; Sidak's multiple comparisons test; p=0.52) or after LTP (WT=39.43 +/- 2.55 μm^2; n=14; Q37A/R38A=45.73 +/- 5.35 μm^2; n=14; ANOVA; Sidak's multiple comparisons test; p=0.43).

B. Ratio of the mCherry-Shank3 fluorescence intensity in the PSD : mCherry-Shank3 fluorescence intensity in the dendritic shaft. No significant differences were found between Shank3 WT and Shank3 Q37A/R38A under basal conditions (WT=6.67 +/- 1.54; n=14; Q37A/R38A=10.70 +/- 0.14; n=14; ANOVA; Sidak's multiple comparisons test; p=0.22) or after LTP (WT=7.14 +/- 1.6; n=16; Q37A/R38A=12.10 +/- 2.38; n=13; ANOVA; Sidak's multiple comparisons test; p=0.10).

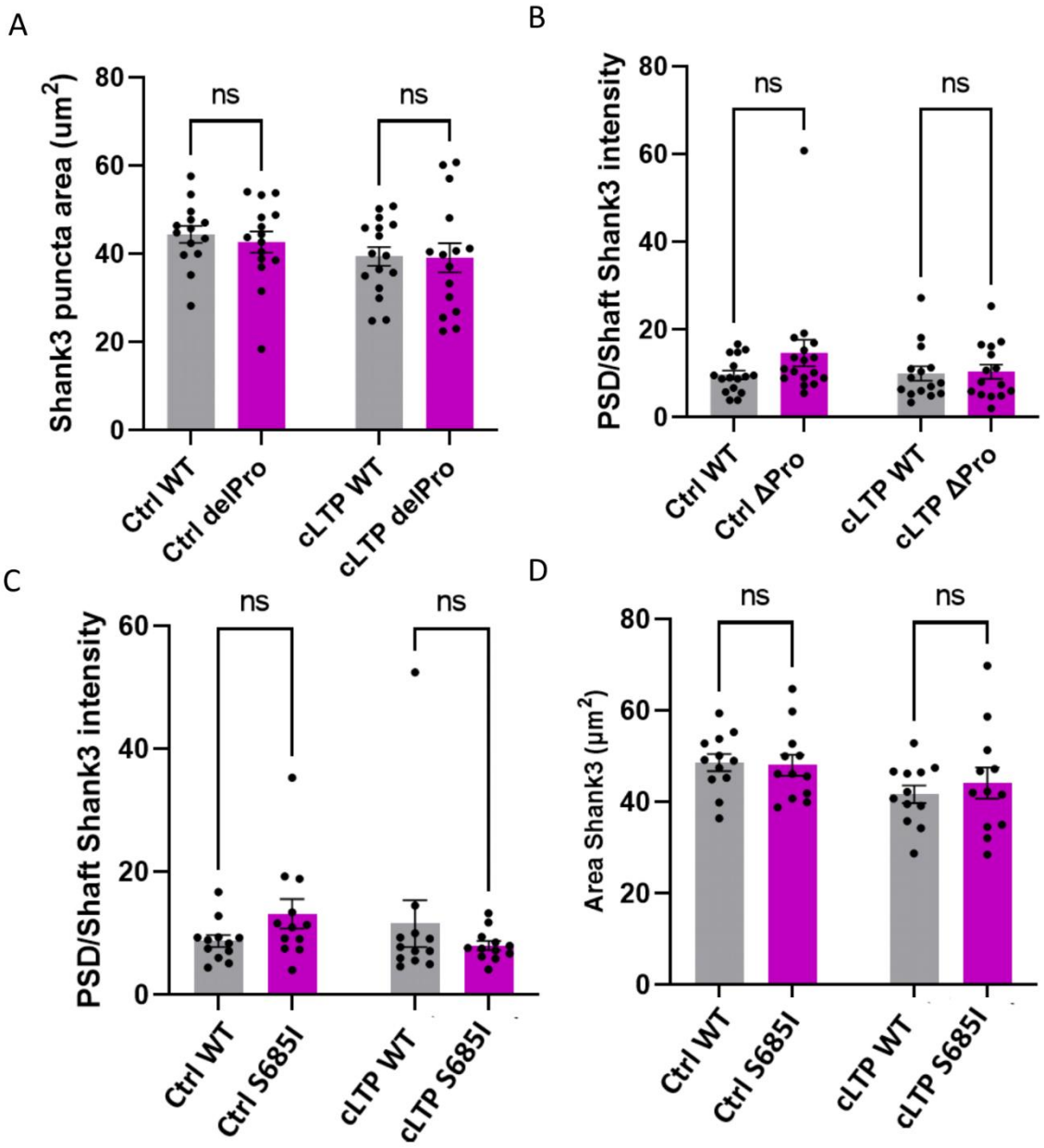

Supplementary figure 3. Shank3 ΔPro and S685I mutations do not disturb Shank3 synaptic targeting.

A. Mean area of Shank3 punctae in the PSDs of neurons transfected with Shank1-3 KD + mCherry-Shank3 WT or Shank1-3 KD + mCherry-Shank3 ΔPro and Homer1c-ALFA. No differences were found between Shank3 WT and Shank3 ΔPro area under basal conditions (WT=44.43 +/- 1.96 μm^2; n=14; ΔPro=42.70 +/- 2.43 μm^2; n=15; ANOVA; Sidak's multiple comparisons test; p=0.98) or after LTP (WT=39.43 +/- 2.13 μm^2; n=16; ΔPro=39.14 +/- 3.32 μm^2; n=15; ANOVA; Sidak's multiple comparisons test; p=0.52).

B. Ratio of the mCherry-Shank3 fluorescence intensity in the PSD: mCherry-Shank3 fluorescence intensity in the dendritic shaft. No significant differences were found between Shank3 WT and Shank3 ΔPro under basal conditions (WT=9.64 +/- 1.02; n=16; ΔPro=14.68 +/- 3.04; n=17; ANOVA; multiple comparisons test; p=0.15) or after LTP (WT=9.98 +/- 1.63; n=15; ΔPro=10.39 +/- 1.65; ANOVA; Sidak's multiple comparisons test; p=0.99).

C. Mean area of Shank3 punctae in the PSDs of neurons transfected with Shank1-3 KD + mCherry-Shank3 WT or Shank1-3 KD + mCherry-Shank3 S685I and Homer1c-ALFA. No

differences were found between Shank3 WT and Shank3 S685I area under basal conditions (WT=48.66 +/- 1.87 µm^2; n=12; S685I= 48.08 +/- 2.31 µm^2; n=12; ANOVA; Sidak's multiple comparisons test; p=0.98) or after LTP (WT=41.71 +/- 1.94 µm^2; n=12; S685I=44.18 +/- 3.39 µm^2; n=12; ANOVA; Sidak's multiple comparisons; p=0.73).

D. Ratio of the mCherry-Shank3 fluorescence intensity in the PSD : mCherry-Shank3 fluorescence intensity in the dendritic shaft. No significant differences were found between Shank3 WT and Shank3 S685I under basal conditions (WT=8,75 +/- 0.97; n=12; S685I=13.17 +/- 2.39; n=12; ANOVA; Sidak's multiple comparisons test; p=0.34) or after LTP (WT=11.56 +/- 3.80; n=12; S685I=8.02 +/- 0.73; n=12; ANOVA; Sidak's multiple comparisons test; p=0.49).

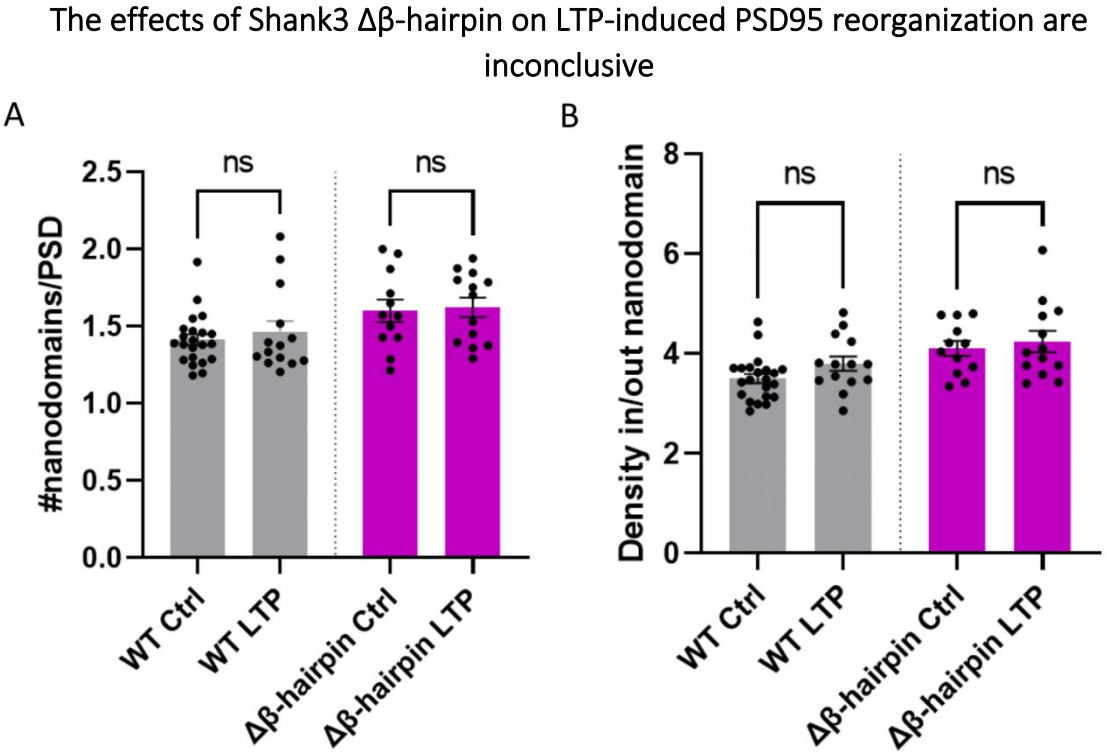

Supplementary figure 4. The effects of the Shank3 Δβ-hairpin mutation on LTP-induced PSD95 reorganization are unclear.

A. Mean number of PSD95 nanodomains per PSD in neurons expressing Shank3r WT or Shank3r Δβ-hairpin after cLTP induction. No significant differences were found in the number of PSD95 nanodomains/PSD after LTP induction compared to the control for re-expression of Shank3r WT (Control=1.41 +/- 0.04; n=22; cLTP=1.46 +/- 0.07; n=14; ANOVA; Sidak's multiple comparisons; p=0.95)or Shank3r Δβ-hairpin (Control=1.60 +/- 0.07; n=12; cLTP=1.62 +/- 0.06; n=13; ANOVA; Sidak's multiple comparisons test; p=0.99).

B. Mean relative density of PSD95 nanodomains after knockdown of Shank1-3 and re-expression of Shank3 WT or Shank3 Δβ-hairpin and cLTP induction. There are no significant differences in the relative density of PSD95 nanodomains after LTP induction compared to the control for re-expression of Shank3 WT (Control=3.5 +/- 0.09; n=22; cLTP=3.80 +/- 0.15; n=14; ANOVA; Sidak's multiple comparisons test; p=0.41) or Shank3 Δβ-hairpin (Control=4.1 +/- 0.15; n=12; cLTP=4.21 +/- 0.21; n=13; p=0.17).

The effects of Shank3 Q37A/R38A, ΔPro and S685I mutations on LTP-induced PSD95 reorganization are inconclusive

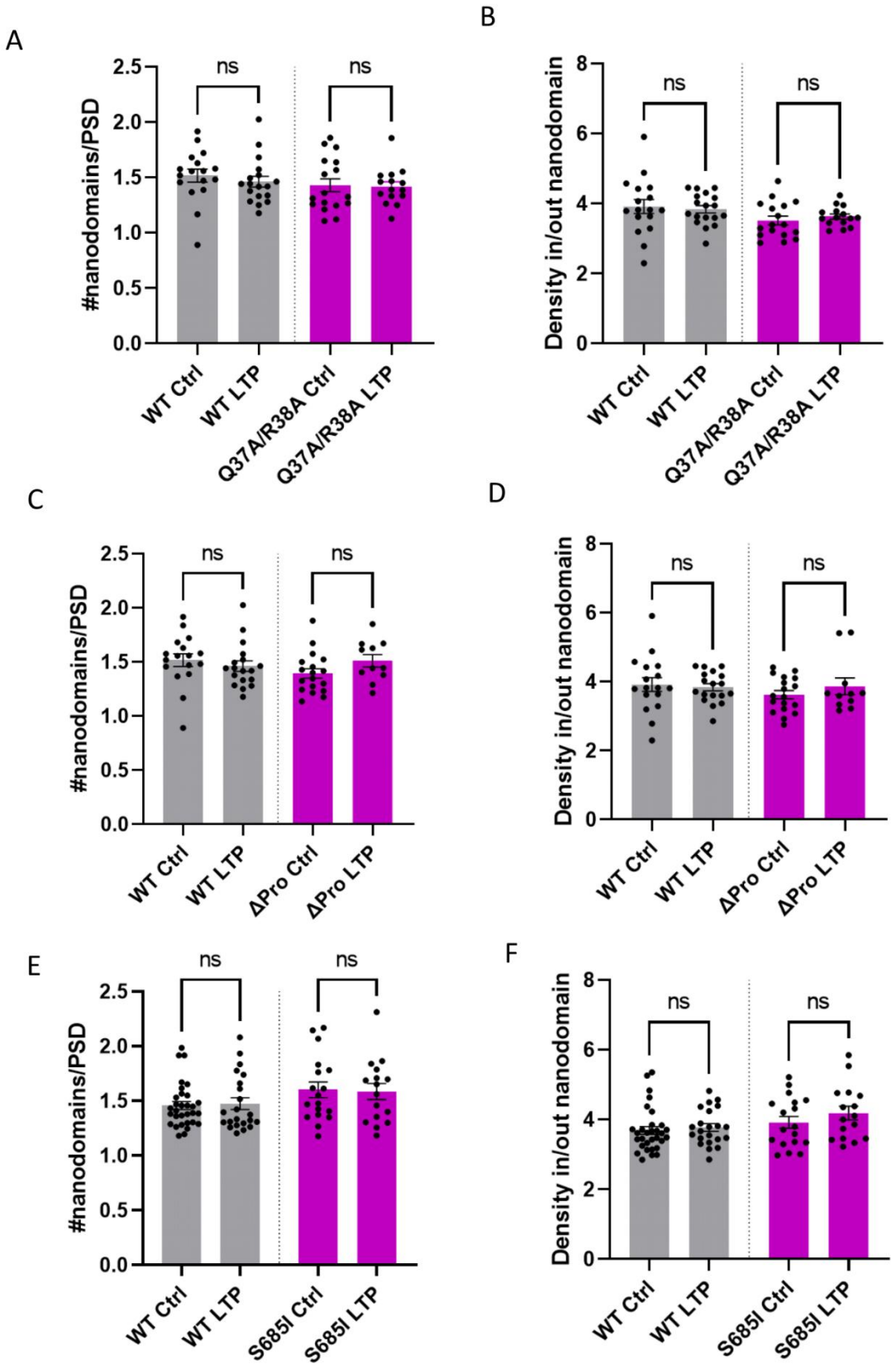

Supplementary figure 5. The effects of the Shank3 ΔPro and S685I mutations on LTP-induced PSD95 reorganization are unclear.

A. Mean number of PSD95 nanodomains per PSD after knockdown of Shank1-3 and re-expression of Shank3 WT or Shank3 Q37A/R38A after cLTP induction. No significant differences were found in the number of PSD95 nanodomains/PSD after LTP induction compared to the control for re-expression of Shank3 WT (Control=1.52 +/- 0.06; n=17; cLTP=1.46 +/- 0.05; n=18; ANOVA; Sidak's multiple comparisons test; p=0.91) or Shank3 Q37A/R38A (Control=1.43 +/- 0.06; n=17; cLTP=1.42 +/- 0.04; n=15; ANOVA; Sidak's multiple comparisons test ; p>0.99).
B. Mean relative density of PSD95 nanodomains after knockdown of Shank1-3 and re-expression of Shank3 WT or Shank3 Δβ-hairpin and cLTP induction. There are no significant differences in the relative density of PSD95 nanodomains after LTP induction compared to the control for re-expression of Shank3 WT (Control=3.91 +/- 0.2; n=17; cLTP=3.84 +/- 0.10; n=18; ANOVA; Sidak's multiple comparisons test; p=0.99) or Shank3 Q37A/R38A (Control=3.52 +/- 0.13; n=17; cLTP=3.63 +/- 0.07; n=15; ANOVA; Sidak's multiple comparisons test ; p=0.97).
C. Mean number of PSD95 nanodomains per PSD after knockdown of Shank1-3 and re-expression of Shank3 WT or Shank3 ΔPro after cLTP induction. No significant differences were found in the number of PSD95 nanodomains/PSD after LTP induction compared to the control for re-expression of Shank3 WT (Control=1.52 +/- 0.06; n=17; cLTP=1.46 +/- 0.05; n=18; ANOVA; Sidak's multiple comparisons test; p=0.90) or Shank3 ΔPro (Control= 1.40 +/- 0.04; n=18; cLTP=1.51 +/- 0.06; n=11; ANOVA; Sidak's multiple comparisons test; p=0.49).
D. Mean relative density of PSD95 nanodomains after knockdown of Shank1-3 and re-expression of Shank3 WT or Shank3 ΔPro and cLTP induction. There are no significant differences in the relative density of PSD95 nanodomains after LTP induction compared to the control for re-expression of Shank3 WT (Control=3.92 +/- 0.2; n=17; cLTP=3.84 +/- 0.10; n=18; ANOVA; Sidak's multiple comparisons test; p=0.99) or Shank3 ΔPro (Control=3.62 +/- 0.12; n=18; cLTP=3.87 +/- 0.24; n=11; ANOVA; Sidak's multiple comparisons test ; p=0.80).
E. Mean number of PSD95 nanodomains per PSD after knockdown of Shank1-3 and re-expression of Shank3 WT or Shank3 S685I after cLTP induction. No significant differences were found in the number of PSD95 nanodomains/PSD after LTP induction compared to the control for re-expression of Shank3 WT (Control= 1.46 +/- 0.04; n=31; cLTP=1.48 +/- 0.05; n=22; ANOVA; Sidak's multiple comparisons test; p=0.99) or Shank3 S685I (Control=1.6 +/- 0.07; n=18; cLTP=1.59 +/- 0.07; n=16; ANOVA; Sidak's multiple comparisons test; p>0.99).
F. Mean relative density of PSD95 nanodomains after knockdown of Shank1-3 and re-expression of Shank3 WT or Shank3 S685I and cLTP induction. There are no significant differences in the relative density of PSD95 nanodomains after LTP induction compared to the control for re-expression of Shank3 WT (Control=3.69 +/- 0.11; n=31; cLTP=3.77 +/- 0.11; n=22; ANOVA; Sidak's multiple comparisons test; p=0.98) or Shank3 S685I (Control=3.92 +/- 0.17; n=18; cLTP=4.18 +/- 0.20; n=16; ANOVA; Sidak's multiple comparisons test; p=0.21).

LatB treatment & wash-out might lead to a decrease in actin dynamics

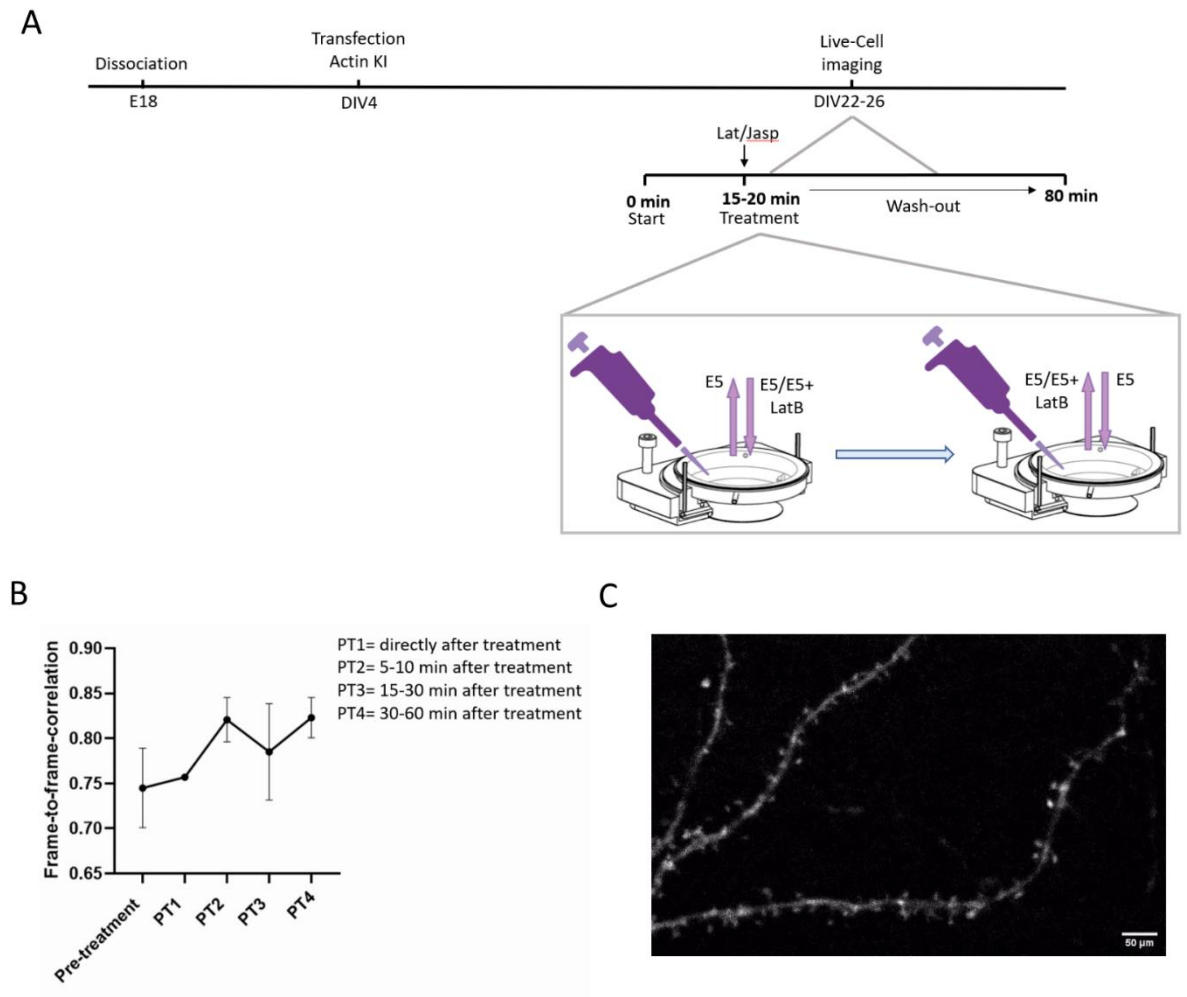

Supplementary figure 6. Actin dynamics may be decreased after treatment with LatB and drug wash-out.

A. Schematic overview of the experimental set-up. Rat hippocampal neurons are transfected with ORANGE actin KI that labels endogenous actin (F-actin and G-actin) with… Then, the transfected neurons were live-cell imaged (DIV22-26) on the spinning disk microscope for 75 minutes (5 minute interval between imaging). For the first 15 minutes, the neurons were kept in 500 µL E5 medium. Then, the medium was switched out for 500 µL E5 with 1 µM LatB for 5 minutes. After these 5 minutes, the medium with LatB was again exchanged for normal E5 minutes. Finally, the neurons were imaged for an additional 60 minutes.

B. Mean frame-to-frame correlation for the actin- intensity. The frame-to-frame correlation was obtained by measuring the integrated densities (InDen) for each frame per PSD. Differences in the InDen between frames were obtained by subtracting each frame (t_x) from the previous (t_x-1). Finally, the frame-to-frame correlation was calculated with the formula: (InDen t_x−[InDen t_x−InDen t_{x-1}])/InDen $t_{x..}$

C. Representative image of dendrites of neurons transfected with the ORANGE β-actin KI.

References

Arons, M.H., Thynne, C.J., Grabrucker, A.M., Li, D., Schoen, M., Cheyne, J.E., Boeckers, T.M., Montgomery, J.M. & Garner, C.C. (2012). Autism-Associated Mutations in ProSAP2/Shank3 Impair Synaptic Transmission and Neurexin-Neuroligin-Mediated Transsynaptic Signalling. *Journal of Neuroscience, 32* (43), 14966-14978. https://doi.org/10.1523/jneurosci.2215-122.2012

Bats, C., Groc, L. & Choquet, D. (2007). The Interaction between Stargazin and PSD-95 Regulates AMPA Receptor Surface Trafficking. *Neuron*, *53*(5), 719–734. https://doi.org/10.1016/j.neuron.2007.01.030

Bosch, M., Castro, J., Saneyoshi, T., Matsuno, H., Sur, M. & Hayashi, Y. (2014). Structural and Molecular Remodeling of Dendritic Spine Substructures during Long-Term Potentiation. *Neuron*, *82*(2), 444–459. https://doi.org/10.1016/j.neuron.2014.03.021

Boucher, J., Kröger, H. & Sík, A. (2010). Realistic modelling of receptor activation in hippocampal excitatory synapses: analysis of multivesicular release, release location, temperature and synaptic cross-talk. *Brain Structure and Function*, *215*(1), 49–65. https://doi.org/10.1007/s00429-010-0273-x

Bozdagi, O., Sakurai, T., Papapetrou, D., Wang, X., Dickstein, D. L., Takahashi, N., Kajiwara, Y., Yang, M., Katz, A. M., Scattoni, M. L., Harris, M. J., Saxena, R., Silverman, J. L., Crawley, J. N., Zhou, Q., Hof, P. R. & Buxbaum, J. D. (2010). Haploinsufficiency of the autism-associated Shank3 gene leads to deficits in synaptic function, social interaction, and social communication. *Molecular Autism*, *1*(1). https://doi.org/10.1186/2040-2392-1-15

Broadhead, M. J., Horrocks, M. H., Zhu, F., Muresan, L., Benavides-Piccione, R., DeFelipe, J., Fricker, D., Kopanitsa, M. V., Duncan, R. R., Klenerman, D., Komiyama, N. H., Lee, S. F. & Grant, S. G. N. (2016). PSD95 nanoclusters are postsynaptic building blocks in hippocampus circuits. *Scientific Reports*, *6*(1). https://doi.org/10.1038/srep24626

Bromley-Brits, K., Deng, Y. & Song, W. (2011). Morris Water Maze Test for Learning and Memory Deficits in Alzheimer's Disease Model Mice. *Journal of Vis ualized Experiments*, *53*. https://doi.org/10.3791/2920

Chen, J. H., Kellner, Y., Zagrebelsky, M., Grunwald, M., Korte, M. & Walla, P. J. (2015). Two-Photon Correlation Spectroscopy in Single Dendritic Spines Reveals Fast Actin Filament Reorganization during Activity-Dependent Growth. *PLOS ONE*, *10*(5), e0128241. https://doi.org/10.1371/journal.pone.0128241

Compans, B., Camus, C., Kallergi, E., Sposini, S., Martineau, M., Butler, C., Kechkar, A., Klaassen, R. V., Retailleau, N., Sejnowski, T. J., Smit, A. B., Sibarita, J. B., Bartol, T. M., Perrais, D., Nikoletopoulou, V., Choquet, D. & Hosy, E. (2021). NMDAR-dependent long-term depression is associated with increased short term plasticity through autophagy mediated loss of PSD-95. *Nature Communications*, *12*(1). https://doi.org/10.1038/s41467-021-23133-9

Craven, S. E., El-Husseini, A. E. & Bredt, D. S. (1999). Synaptic Targeting of the Postsynaptic Density Protein PSD-95 Mediated by Lipid and Protein Motifs. *Neuron*, *22*(3), 497–509. https://doi.org/10.1016/s0896-6273(00)80705-9

Durand, C. M., Betancur, C., Boeckers, T. M., Bockmann, J., Chaste, P., Fauchereau, F., Nygren, G., Rastam, M., Gillberg, I. C., Anckarsäter, H., Sponheim, E., Goubran-Botros, H., Delorme, R., Chabane,

N., Mouren-Simeoni, M. C., de Mas, P., Bieth, E., Rogé, B., Héron, D., . . . Bourgeron, T. (2006). Mutations in the gene encoding the synaptic scaffolding protein SHANK3 are associated with autism spectrum disorders. *Nature Genetics*, *39*(1), 25–27. https://doi.org/10.1038/ng1933

El-Husseini, A. E., Craven, S. E., Chetkovich, D. M., Firestein, B. L., Schnell, E., Aoki, C. & Bredt, D. S. (2000). Dual Palmitoylation of Psd-95 Mediates Its Vesiculotubular Sorting, Postsynaptic Targeting, and Ion Channel Clustering. *Journal of Cell Biology*, *148*(1), 159–172. https://doi.org/10.1083/jcb.148.1.159

Fonseca, R. (2012). Activity-dependent actin dynamics are required for the maintenance of long-term plasticity and for synaptic capture. *European Journal of Neuroscience*, *35*(2), 195–206. https://doi.org/10.1111/j.1460-9568.2011.07955.x

Franks, K. M., Stevens, C. F. & Sejnowski, T. J. (2003). Independent Sources of Quantal Variability at Single Glutamatergic Synapses. *The Journal of Neuroscience*, *23*(8), 3186–3195. https://doi.org/10.1523/jneurosci.23-08-03186.2003

Fukata, Y., Dimitrov, A., Boncompain, G., Vielemeyer, O., Perez, F. & Fukata, M. (2013). Local palmitoylation cycles define activity-regulated postsynaptic subdomains. *Journal of Cell Biology*, *202*(1), 145–161. https://doi.org/10.1083/jcb.201302071

Fukazawa, Y., Saitoh, Y., Ozawa, F., Ohta, Y., Mizuno, K. & Inokuchi, K. (2003). Hippocampal LTP Is Accompanied by Enhanced F-Actin Content within the Dendritic Spine that Is Essential for Late LTP Maintenance In Vivo. *Neuron*, *38*(3), 447–460. https://doi.org/10.1016/s0896-6273(03)00206-x

García-Nafría, J., Watson, J. F. & Greger, I. H. (2016). IVA cloning: A single-tube universal cloning system exploiting bacterial In Vivo Assembly. *Scientific Reports*, *6*(1). https://doi.org/10.1038/srep27459

Gierut, J. J., Jacks, T. E. & Haigis, K. M. (2014). Strategies to Achieve Conditional Gene Mutation in Mice. *Cold Spring Harbor Protocols*, *2014*(4),069807. https://doi.org/10.1101/pdb.top069807

Hayashi, Y., Shi, S. H., Esteban, J. A., Piccini, A., Poncer, J. C. & Malinow, R. (2000). Driving AMPA Receptors into Synapses by LTP and CaMKII: Requirement for GluR1 and PDZ Domain Interaction. *Science*, *287*(5461), 2262–2267. https://doi.org/10.1126/science.287.5461.2262

Hill, C. L. & Stephens, G. J. (2020). An Introduction to Patch Clamp Recording. *Patch Clamp Electrophysiology*, 1–19. https://doi.org/10.1007/978-1-0716-0818-0_1

Holzinger, A. (2009). Jasplakinolide: An Actin-Specific Reagent that Promotes Actin Polymerization. *Cytoskeleton Methods and Protocols*, 71–87. https://doi.org/10.1007/978-1-60761-376-3_4

Hruska, M., Henderson, N., Le Marchand, S. J., Jafri, H. & Dalva, M. B. (2018). Synaptic nanomodules underlie the organization and plasticity of spine synapses. *Nature Neuroscience*, *21*(5), 671–682. https://doi.org/10.1038/s41593-018-0138-9

Jeong, J., Li, Y. & Roche, K. W. (2021). CaMKII Phosphorylation Regulates Synaptic Enrichment of Shank3. *eneuro*, *8*(3), ENEURO.0481-20.2021. https://doi.org/10.1523/eneuro.0481-20.2021

Katrukha E. (2020). Detection of Molecules (DoM) plugin for ImageJ, v1.2.1, Zenodo, doi:10.5281/zenodo.4281069

Katrukha E. (2021). ComDet plugin for ImageJ, v0.5.5, Zenodo, doi:10.5281/zenodo.4281064

Keller, R., Basta, R., Salerno, L. & Elia, M. (2017). Autism, epilepsy, and synaptopathies: a not rare association. *Neurological Sciences*, *38*(8), 1353–1361. https://doi.org/10.1007/s10072-017-2974-x

Kim, C. H. & Lisman, J. E. (1999). A Role of Actin Filament in Synaptic Transmission and Long-Term Potentiation. *The Journal of Neuroscience*, *19*(11), 4314–4324. https://doi.org/10.1523/jneurosci.19-11-04314.1999

Kouser, M., Speed, H. E., Dewey, C. M., Reimers, J. M., Widman, A. J., Gupta, N., Liu, S., Jaramillo, T. C., Bangash, M., Xiao, B., Worley, P. F. & Powell, C. M. (2013). Loss of Predominant Shank3 Isoforms Results in Hippocampus-Dependent Impairments in Behavior and Synaptic Transmission. *Journal of Neuroscience*, *33*(47), 18448–18468. https://doi.org/10.1523/jneurosci.3017-13.2013

Krucker, T., Siggins, G. R. & Halpain, S. (2000). Dynamic actin filaments are required for stable long-term potentiation (LTP) in area CA1 of the hippocampus. *Proceedings of the National Academy of Sciences*, *97*(12), 6856–6861. https://doi.org/10.1073/pnas.100139797

Lilja, J., Zacharchenko, T., Georgiadou, M., Jacquemet, G., Franceschi, N., Peuhu, E., Hamidi, H., Pouwels, J., Martens, V., Nia, F., Beifuss, M., Boeckers, T., Kreienkamp, H. J., Barsukov, I. & Ivaska, J. (2017). SHANK proteins limit integrin activation by directly interacting with Rap1 and R-Ras. *Nature Cell Biology*, *19*(4), 292–305. https://doi.org/10.1038/ncb3487

Lisman, J., Yasuda, R. & Raghavachari, S. (2012). Mechanisms of CaMKII action in long-term potentiation. *Nature Reviews Neuroscience*, *13*(3), 169–182. https://doi.org/10.1038/nrn3192

Lynch, G., Larson, J., Kelso, S., Barrionuevo, G. & Schottler, F. (1983). Intracellular injections of EGTA block induction of hippocampal long-term potentiation. *Nature*, *305*(5936), 719–721. https://doi.org/10.1038/305719a0

MacDermott, A. B., Mayer, M. L., Westbrook, G. L., Smith, S. J. & Barker, J. L. (1986). NMDA-receptor activation increases cytoplasmic calcium concentration in cultured spinal cord neurones. *Nature*, *321*(6069), 519–522. https://doi.org/10.1038/321519a0

MacGillavry, H. D., Kerr, J. M., Kassner, J., Frost, N. A. & Blanpied, T. A. (2015). Shank-cortactin interactions control actin dynamics to maintain flexibility of neuronal spines and synapses. *European Journal of Neuroscience*, *43*(2), 179–193. https://doi.org/10.1111/ejn.13129

MacGillavry, H., Song, Y., Raghavachari, S. & Blanpied, T. (2013). Nanoscale Scaffolding Domains within the Postsynaptic Density Concentrate Synaptic AMPA Receptors. *Neuron*, *78*(4), 615–622. https://doi.org/10.1016/j.neuron.2013.03.009

Makino, H. & Malinow, R. (2009). AMPA Receptor Incorporation into Synapses during LTP: The Role of Lateral Movement and Exocytosis. *Neuron*, *64*(3), 381–390. https://doi.org/10.1016/j.neuron.2009.08.035

Martin Ester, Hans-Peter Kriegel, Jörg Sander & Xiaowei Xu. (1996). A density-based algorithm for discovering clusters in large spatial Databases with Noise. *Knowledge Discovery and Data Mining*, 226–231.

Molnar, E. (2011). Long-term potentiation in cultured hippocampal neurons. *Seminars in Cell & Developmental Biology, 22* (5), 506-513. https://doi.ort/10.1016/j.semcdb.2011.07.017

Mizui, T., Sekino, Y., Yamazaki, H., Ishizuka, Y., Takahashi, H., Kojima, N., Kojima, M. & Shirao, T. (2014). Myosin II ATPase Activity Mediates the Long-Term Potentiation-Induced Exodus of Stable F-Actin Bound by Drebrin A from Dendritic Spines. *PLoS ONE*, *9*(1), e85367. https://doi.org/10.1371/journal.pone.0085367

Morton, W. M., Ayscough, K. R. & McLaughlin, P. J. (2000). Latrunculin alters the actin-monomer subunit interface to prevent polymerization. *Nature Cell Biology*, *2*(6), 376–378. https://doi.org/10.1038/35014075

Nair, D., Hosy, E., Petersen, J. D., Constals, A., Giannone, G., Choquet, D. & Sibarita, J. B. (2013). Super-Resolution Imaging Reveals That AMPA Receptors Inside Synapses Are Dynamically Organized in Nanodomains Regulated by PSD95. *Journal of Neuroscience*, *33*(32), 13204–13224. https://doi.org/10.1523/jneurosci.2381-12.2013

Naisbitt, S., Kim, E., Tu, J. C., Xiao, B., Sala, C., Valtschanoff, J., Weinberg, R. J., Worley, P. F. & Sheng, M. (1999). Shank, a Novel Family of Postsynaptic Density Proteins that Binds to the NMDA Receptor/PSD-95/GKAP Complex and Cortactin. *Neuron*, *23*(3), 569–582. https://doi.org/10.1016/s0896-6273(00)80809-0

Nakahata, Y. & Yasuda, R. (2018). Plasticity of Spine Structure: Local Signaling, Translation and Cytoskeletal Reorganization. *Frontiers in Synaptic Neuroscience*, *10*. https://doi.org/10.3389/fnsyn.2018.00029

Obi-Nagata, K., Temma, Y. & Hayashi-Takagi, A. (2019). Synaptic functions and their disruption in schizophrenia: From clinical evidence to synaptic optogenetics in an animal model. *Proceedings of the Japan Academy, Series B*, *95*(5), 179–197. https://doi.org/10.2183/pjab.95.014

Okamoto, K. I., Nagai, T., Miyawaki, A. & Hayashi, Y. (2004). Rapid and persistent modulation of actin dynamics regulates postsynaptic reorganization underlying bidirectional plasticity. *Nature Neuroscience*, *7*(10), 1104–1112. https://doi.org/10.1038/nn1311

Perfitt, T. L., Wang, X., Dickerson, M. T., Stephenson, J. R., Nakagawa, T., Jacobson, D. A. & Colbran, R. J. (2020). Neuronal L-Type Calcium Channel Signaling to the Nucleus Requires a Novel CaMKIIα-Shank3 Interaction. *The Journal of Neuroscience*, *40*(10), 2000–2014. https://doi.org/10.1523/jneurosci.0893-19.2020

Quadros, R. M., Miura, H., Harms, D. W., Akatsuka, H., Sato, T., Aida, T., Redder, R., Richardson, G. P., Inagaki, Y., Sakai, D., Buckley, S. M., Seshacharyulu, P., Batra, S. K., Behlke, M. A., Zeiner, S. A., Jacobi, A. M., Izu, Y., Thoreson, W. B., Urness, L. D., . . . Gurumurthy, C. B. (2017). Easi-CRISPR: a robust method for one-step generation of mice carrying conditional and insertion alleles using long ssDNA donors and CRISPR ribonucleoproteins. *Genome Biology*, *18*(1). https://doi.org/10.1186/s13059-017-1220-4

Qin, W., Dion, S. L., Kutny, P. M., Zhang, Y., Cheng, A. W., Jillette, N. L., Malhotra, A., Geurts, A. M., Chen, Y. G. & Wang, H. (2015). Efficient CRISPR/Cas9-Mediated Genome Editing in Mice by Zygote Electroporation of Nuclease. *Genetics*, *200*(2), 423–430. https://doi.org/10.1534/genetics.115.176594

Raghavachari, S. & Lisman, J. E. (2004). Properties of Quantal Transmission at CA1 Synapses. *Journal of Neurophysiology*, *92*(4), 2456–2467. https://doi.org/10.1152/jn.00258.2004

Regehr, W. G. & Tank, D. W. (1990). Postsynaptic NMDA receptor-mediated calcium accumulation in hippocampal CA1 pyramidal cell dendrites. *Nature*. https://doi.org/10.1038/345807a0

Sala, C., Piëch, V., Wilson, N. R., Passafaro, M., Liu, G. & Sheng, M. (2001). Regulation of Dendritic Spine Morphology and Synaptic Function by Shank and Homer. *Neuron*, *31*(1), 115–130. https://doi.org/10.1016/s0896-6273(01)00339-7

Salomaa, S. I., Miihkinen, M., Kremneva, E., Paatero, I., Lilja, J., Jacquemet, G., Vuorio, J., Antenucci, L., Kogan, K., Hassani Nia, F., Hollos, P., Isomursu, A., Vattulainen, I., Coffey, E. T., Kreienkamp, H. J., Lappalainen, P. & Ivaska, J. (2021). SHANK3 conformation regulates direct actin binding and crosstalk with Rap1 signaling. *Current Biology*, *31*(22), 4956-4970.e9. https://doi.org/10.1016/j.cub.2021.09.022

Sarowar, T. & Grabrucker, A. M. (2016). Actin-Dependent Alterations of Dendritic Spine Morphology in Shankopathies. *Neural Plasticity*, *2016*, 1–15. https://doi.org/10.1155/2016/8051861

Scheefhals, N., Catsburg, L. A., Westerveld, M. L., Blanpied, T. A., Hoogenraad, C. C. & MacGillavry, H. D. (2019). Shank Proteins Couple the Endocytic Zone to the Postsynaptic Density to Control Trafficking and Signaling of Metabotropic Glutamate Receptor 5. *Cell Reports*, *29*(2), 258-269.e8. https://doi.org/10.1016/j.celrep.2019.08.102

Scheefhals, N. & MacGillavry, H. D. (2018). Functional organization of postsynaptic glutamate receptors. *Molecular and Cellular Neuroscience*, *91*, 82–94. https://doi.org/10.1016/j.mcn.2018.05.002

Schnell, E., Sizemore, M., Karimzadegan, S., Chen, L., Bredt, D. S. & Nicoll, R. A. (2002). Direct interactions between PSD-95 and stargazin control synaptic AMPA receptor number. *Proceedings of the National Academy of Sciences*, *99*(21), 13902–13907. https://doi.org/10.1073/pnas.172511199

Serweta, A.K., Droogers, W.J., MacGillavry, H.D. (2021) Scaffold nanodomains in the postsynaptic density re-organize during long-term potentiation. Division of Cell Biology, Neurobiology and Biophysics, Utrecht University. Unpublished.

Shi, S. H., Hayashi, Y., Petralia, R. S., Zaman, S. H., Wenthold, R. J., Svoboda, K. & Malinow, R. (1999). Rapid Spine Delivery and Redistribution of AMPA Receptors After Synaptic NMDA Receptor Activation. *Science*, *284*(5421), 1811–1816. https://doi.org/10.1126/science.284.5421.1811

Tang, A. H., Chen, H., Li, T. P., Metzbower, S. R., MacGillavry, H. D. & Blanpied, T. A. (2016). A trans-synaptic nanocolumn aligns neurotransmitter release to receptors. *Nature*, *536*(7615), 210–214. https://doi.org/10.1038/nature19058

Tu, J. C., Xiao, B., Naisbitt, S., Yuan, J. P., Petralia, R. S., Brakeman, P., Doan, A., Aakalu, V. K., Lanahan, A. A., Sheng, M. & Worley, P. F. (1999). Coupling of mGluR/Homer and PSD-95 Complexes by the Shank Family of Postsynaptic Density Proteins. *Neuron*, *23*(3), 583–592. https://doi.org/10.1016/s0896-6273(00)80810-7

Uruno, T., Liu, J., Zhang, P., Fan, Y. X., Egile, C., Li, R., Mueller, S. C. & Zhan, X. (2001). Activation of Arp2/3 complex-mediated actin polymerization by cortactin. *Nature Cell Biology*, *3*(3), 259–266. https://doi.org/10.1038/35060051

Wang, L., Pang, K., Han, K., Adamski, C. J., Wang, W., He, L., Lai, J. K., Bondar, V. V., Duman, J. G., Richman, R., Tolias, K. F., Barth, P., Palzkill, T., Liu, Z., Holder, J. L. & Zoghbi, H. Y. (2019). An autism-

linked missense mutation in SHANK3 reveals the modularity of Shank3 function. *Molecular Psychiatry*, *25*(10), 2534–2555. https://doi.org/10.1038/s41380-018-0324-x

Weaver, A. M., Karginov, A. V., Kinley, A. W., Weed, S. A., Li, Y., Parsons, J. & Cooper, J. A. (2001). Cortactin promotes and stabilizes Arp2/3-induced actin filament network formation. *Current Biology*, *11*(5), 370–374. https://doi.org/10.1016/s0960-9822(01)00098-7

Wiesner, T., Bilodeau, A., Bernatchez, R., Deschênes, A., Raulier, B., De Koninck, P. & Lavoie-Cardinal, F. (2020). Activity-Dependent Remodeling of Synaptic Protein Organization Revealed by High Throughput Analysis of STED Nanoscopy Images. *Frontiers in Neural Circuits*, *14*. https://doi.org/10.3389/fncir.2020.00057

Willems, J., de Jong, A. P. H., Scheefhals, N., Mertens, E., Catsburg, L. A. E., Poorthuis, R. B., de Winter, F., Verhaagen, J., Meye, F. J. & MacGillavry, H. D. (2020). ORANGE: A CRISPR/Cas9-based genome editing toolbox for epitope tagging of endogenous proteins in neurons. *PLOS Biology*, *18*(4), e3000665. https://doi.org/10.1371/journal.pbio.3000665

Wilson, H. L. (2003). Molecular characterisation of the 22q13 deletion syndrome supports the role of haploinsufficiency of SHANK3/PROSAP2 in the major neurological symptoms. *Journal of Medical Genetics*, *40*(8), 575–584. https://doi.org/10.1136/jmg.40.8.575

Won, H., Lee, H. R., Gee, H. Y., Mah, W., Kim, J. I., Lee, J., Ha, S., Chung, C., Jung, E. S., Cho, Y. S., Park, S. G., Lee, J. S., Lee, K., Kim, D., Bae, Y. C., Kaang, B. K., Lee, M. G. & Kim, E. (2012). Autistic-like social behaviour in Shank2-mutant mice improved by restoring NMDA receptor function. *Nature*, *486*(7402), 261–265. https://doi.org/10.1038/nature11208

Zeng, M., Shang, Y., Guo, T., He, Q., Yung, W. H., Liu, K. & Zhang, M. (2016). A binding site outside the canonical PDZ domain determines the specific interaction between Shank and SAPAP and their function. *Proceedings of the National Academy of Sciences*, *113*(22). https://doi.org/10.1073/pnas.1523265113